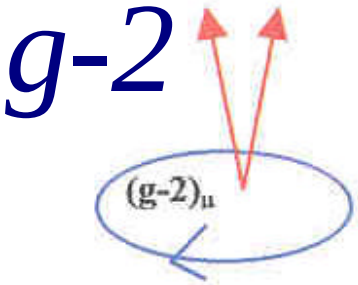

Brookhaven National Laboratory

Brookhaven Science Associates

Upton, New York 11973

Muon g-2 Note No. 390

Title: **Analysis of the 1999 Muon Spin precession Data**

Author(s): **Gerco Onderwater**

Affiliation: **University of Illinois**

Date: **March 28, 2001**

Analysis of the 1999 Muon Spin Precession Data

Gerco Onderwater

University of Illinois

Abstract

The results of an ω_a analysis based on the G2Too production and a multi-parameter fitting method are discussed. The methods used to determine several parameters which are not fitted directly are presented and discussed. The final result, *excluding* any corrections, is $\omega_a/2\pi = 229,072.60 \pm 0.28\,(stat.) \pm 0.02\,(syst.)$ Hz, or $R = 143.30 \pm 1.23\,(stat.) \pm 0.08\,(syst.)$ (including an offset of 23.7).

1 Introduction

In the following document, the results and methods used to obtain the muon spin precession frequency ω_a from the 1999 $(g-2)$ data produced by G2Too are presented and discussed. Several essential preparational steps in the analysis are discussed as well.

This document is split in the following items:

- Data Preparation
  - Data Selection
  - Detector Calibration
  - Randomization
  - Pileup Correction
  - Histogramming
  - Versions of MilliFitter
- Fitting
  - Nominal Part
  - Pileup Part
  - Coherent Betatron Oscillations
  - Energy Scale Changes
  - Muon Losses
  - Summary

- Results
  - Fixed Parameters
    - Pileup Related Parameters
    - CBO Related Parameters
    - Muon Loss Related Parameters
  - Floating Parameters
    - Magnitude and Stability of χ^2
    - Start Time Stability
    - Residuals at Final Start Times
    - Consistency among Detectors
  - Systematic Errors
    - Energy Scale Corrections
    - Coherent Betatron Oscillations
    - Muon Losses
    - Fitting Start Time
    - Pileup Subtraction
    - Other sources and Summary
- Conclusion

2 Data Preparation

2.1 *Data Selection*

For this analysis, the runs selected by Ernst were used as mailed to the g2offline mailing list on July 6th including the additional remarks that were mailed on July 9th. Because of well known problems with its WFD, the data for detector 2 is not used in the final analysis. Detector 20 is not used because its position with respect to the ring is different from the other detectors (it was pulled out of the magnet gap by about 3 inches in the 1999 run) which leads to a different acceptance. More important, the balancing of the gains of the PMT on the front and back of this detector was not done correctly, leading to non-linearities in the energy reconstrcution. As suggested by Ernst, detector 18 was discarded for runs in the range 3903 – 4139, and detector 14 for runs 4790 – 4796.

Fill quality control was based on the data recorded for the T0 injection counter, the laser reference WFD and CAMAC ADCs and the quad traces. In the fitted data for the T0 counter, there should be at least one event with an area of more than 100 counts. Proper fitting relies on the correct aligning of the two WFD phases and the succesful fitting of the marker-pulse. The latter condition is of course applied to all WFD related data. Once there is a fill which does not pass these criteria, the entire AGS cycle is left out of further

analysis.

As there are no laser runs included in the list provided by Ernst, checking for the laser to fire should be unnecessary. Nevertheless, the standard check for laser signals is applied. If there are succesfully fitted events from the laser reference WFD or if the CAMAC ADCs have a signal exceeding 100 counts, the fill is omitted from further analysis.

The condition for good quad operation is based on three samples taken from the WFD trace (the 100th, 250th and 1500th). If the difference between the first and second or between the second and third sample deviates by more than 6 counts from the expected value, a quad-spark or discharge is assumed and the fill is discarded from the analysis.

2.2 *Detector Calibration*

The calibration of the detector reponse was done by Long and will be described in his report of the 1999 data analysis. For completeness, the list of gains and time offsets used in this analysis is given in table 11 in the appendix. The time dependence of the gain (*a.k.a.* energy scale changes) was fitted to the data prepared by Long using the pileup subtraction method developped by Cenap *et al.*. The parameterization and fitting results are discussed later.

2.3 *Randomization*

Several sets of histograms were prepared for this analysis. In the early stages of the analysis, event-by-event randomization was employed to eliminate the influence of the fast rotation on the fitting results. The randomization period was taken from Robs presentation at the previous $(g-2)$ collaboration meeting at BNL as $\frac{7114}{7112} \times 149.14337\,\text{ns} = 149.185\,\text{ns}$. The randomization was done by generating a random time offset between $-\frac{1}{2}$ and $\frac{1}{2}$ times this period, so that the average time offset was zero. In the final stage, fill-by-fill randomization was used to allow pileup correction. The random number generator used was the Mersenne-Twistor version[1], which has a period of $2^{19937} - 1 \simeq 10^{6000}$.

In a single pass through the data, a systematic error related to the statistical accuracy of the randomization is expected. It was found in this analysis , that the magnitude of this error is about 8% of the statistical error of the data itself. This error can be reduced by repeating the procedure for different sequences of random numbers and averaging the fitting results obtained for each sequence.

Randomization with multiple sequences was done in a single pass through the data. For a given run, a single random number generator was used, the seed of which was set to a

thousand times the run number. For each fill and each detector, a set of ten random time offsets was generated and added to each positron time on a fill-by-fill basis.

Unfortunately, there is no mathematically rigorous proof available in the $(g-2)$ community that averaging the fitting results is allowed, since after all the data is strongly correlated. However, emperically it has been demonstrated that no significant systematic bias is introduced.

2.4 *Pileup Correction*

The method used to eliminate the contribution of pileup is similar to the standard technique used to correct for random coincidence in timing experiments. The method is based on the use of a software deadtime to create artificial pileup. The problems in creating artificial pileup is the hardware threshold of the WFD. This problem is in part overcome by the extended length of a digitization island, which leads to a zero-threshold for all samples but the ones that sample the pulse that triggered the WFD.

The extend of the island was studied carefully and it was shown that the pulse finder is fully efficient upto 17 ns *before* and more than 40 ns *after* the pulse that triggered the WFD. This allows for software deadtimes upto 17 ns and eliminates the need to count combinations of which the first pulse is below the hardware threshold twice.

In practice, I loop over individually fitted events that have an energy above the software threshold of about 250 MeV. For each event, the times of succesive events are examined. If the next event(s) are within the deadtime, their energies are added to that of the first event (with a 94% pileup correction factor) and their times are averaged after weighting by energy. No time offsets are applied to avoid the introducing false phase shifts. Once no other events are found in the vicinity of the ones added together, the time and energy of this summed events is used for further analysis. Most of the time there will be a single events only, so that the summed energy and averaged time are simply the energy and time of this single event.

The amount of two particle pileup created in this manner is linealy proportional to the deadtime applied. Pileup correction is done by preparing two data sets with different deadtimes, so that the amount of pileup in each is different. So the number of counts N_i in each is given by the true number of events N plus the number of pileup events per unit of deadtime P times the deadtime ΔT_i, $N_i = N + P * \Delta T_i$. With two different values for ΔT_i the true number of events is obtained straightforwardly by solving the two linear equations with two unknowns:

$$N = \frac{\Delta T_2 N_1 - \Delta T_1 N_2}{\Delta T_2 - \Delta T_1} \tag{1}$$

$$P = \frac{N_2 - N1}{\Delta T_2 - \Delta T_1} \tag{2}$$

Similarly, higher order pileup can be studied when more deadtimes are used.

A point of interest was the choice of the deadtimes. First, the smallest of the two deadtimes should be kept a small as possible. For G2Too, the recommended deadtime is 5 ns[2]. The choice of the second deadtime of 10 ns is motiviated by two considerations. First, the difference between the two deadtimes is equal to the first deadtime, which minimizes the extrapolation error. Secondly, the choice of a deadtime that is a multiple of the digitization interval of the WFD prevents any effect caused irregulaties within this interval (*e.g.* gain modulation) and related effects.

A problem in eliminating pileup is the error propagation. A first order correction is made in calculating the χ^2 during the minimization along the procedure lined out in a recent $(g-2)$-note[7]. Because of the larger deadtime in G2Too, the amplification is scaled accordingly:

$$\chi_i^2 = \frac{(N_i - f(t_i))^2}{f(t_i) \times \left(1 + 0.0343 * e^{\frac{-t_i}{64400}}\right)} \tag{3}$$

At very early times, this leads to a 3.5% change in the local χ^2.

2.5 *Histogramming*

In Root versions lower than 2.25, the bin boundary calculation is based on single precision floating point arithmatics. By our request, that was changed in version 2.25. For the present analysis, version 2.23 was used. To avoid round-off errors, the time used to fill the histogram was derandomized using double precision arithmatics. Similarly, double precision is used in the fitting routines to calculate the bin-centers.

To avoid rounding errors, in the second stage of the analysis, the bin-width is also kept at an integer value, *viz* 150 ns, instead of at 149.185 ns as was used in the first stage. Moreover, a binwidth which is an integer number of WFD periods is advantageous because it eliminates the beating of a gain variation within the WFD sampling period and the binning.

2.6 *Versions of MilliFitter*

For the resuls presented in this report, the most recent version of MilliFitter is used[2]. The main difference between this version and the one that was used before is the way the uncertainty on individual WFD samples are treated. In the first version, the errors used to calculate the χ^2 for a fit were taken from the spread found when making the average pulse-shapes, scaled with the energy added in quadrature to a constant error for the pedestal. It was found that this leads to a sensitivity for small pulses and the length of the island.

In the present version of MilliFitter, least-squares minimization is used instead of χ^2 minimization (*i.e.* the error is constant for all samples and independent of the amplitude of the pulse). Further, the number of samples from which the least-sqaure is calculated is fixed to eliminate all sensitivity to the length of the island. The samples used are centered about the (guessed) position of the peak.

3 Fitting

The fitting function consists of different parts related to different physical phenomena. In the following few sections, each phenomenon and its parameterization is described. For clarity, the fitted and tuneable parameters are indicated in red. In the description of the data, the following effects are considered:

- normal $(g-2)$ wiggle;
- contribution of pileup;
- modulation due to coherent betatron oscillations;
- changes in the energy scale;
- muon losses.

Most of the parameters that describe these phenomena can be obtained with sufficient precision from independent studies and can be kept fixed while fitting the others.

3.1 *Nominal Part*

The nominal part of the fitting function is the well-know five-parameter function, which in a slightly modified parameterization reads

$$N_0(t) = e^{-kt}\left[N - A_c\cos\omega t + A_s\sin\omega t\right]. \tag{4}$$

Here, $\omega = 2\pi \times 229100 \times 10^{-9} \times (1 - R \times 10^6)$. The reason for this parameterization is that for an infinitely long lifetime $k \to 0$, the parameters N, A_c and A_s are entirely othogonal. In the finite, yet still long compared to $2\pi/\omega$, lifetime case, this will still be mostly true. Moreover, A_c and A_s can vary freely without encountering ambiguities such as when using a phase and an asymmetry. Furthermore, by "pulling" N between the parentheses, the term $N \times A$ that would show up in the usual parameterization can be fitted as a single parameter, which will lead to a faster convergence.

The traditional asymmetry and phase can be derived trivially as

$$A = \frac{\sqrt{{A_c}^2 + {A_s}^2}}{N}; \tag{5}$$

$$dA = \frac{\sqrt{{A_c}^2 d{A_c}^2 + {A_s}^2 d{A_s}^2 + ({A_c}^2 + {A_s}^2)^2 dN^2/N^2}}{\sqrt{{A_c}^2 + {A_s}^2} N}; \tag{6}$$

$$\phi = \arctan \frac{A_s}{A_c}; \tag{7}$$

$$d\phi = \frac{\sqrt{{A_c}^2 d{A_s}^2 + {A_s}^2 d{A_c}^2}}{{A_c}^2 + {A_s}^2}. \tag{8}$$

Note that it is implicitly assumed that the parameters are independent, *i.e.* correlations are ignored.

3.2 *Pileup Part*

The contribution of pileup events is well established at this point[3]. The parameterization used is:

$$N_{pu} = e^{-2kt} \left[N_2 - A_p \cos(\omega t + \phi + \Delta\phi_1) - A_{p2} \cos 2(\omega t + \phi + \Delta\phi_2) \right]. \tag{9}$$

The fitted phase of the normal contribution is indicated with $\phi = \arctan \frac{A_s}{A_c}$ and the $\Delta\phi$'s stand for the phase *differences* between the normal and pileup contributions. Both are fixed when fitting the data. The reason for this is that especially $\Delta\phi_1$ correlates strongly with ω, leading to a doubled statistical error on $(g-2)$. Moreover, they can be estimated more acurately than that they can be fitted, leading to a relatively small systematical error, and a considerably smaller total error. In table 1, some predictions based on the Geant simulation are given.

Also well established is the effect of the fast rotation on the amount of pileup[4]. As with all beam-dynamics related effects, the enhancement of pileup at early times is parameter-

Table 1
Phase difference between normal and pileup wiggles for various energy ranges.

Energy range (GeV)	$\Delta\phi$ (mrad)
1.8 – 3.1	1.6
1.8 – 6.2	28.8
2.0 – 3.1	1.9
2.0 – 6.2	-16.2

ized with a Gaussian time-dependence,

$$\mathcal{F}(t) = 1 + A_c e^{-\frac{1}{2}\left(\frac{t-t_c}{\sigma_c}\right)^2} + A_c^{(2)} e^{-\frac{1}{2}\left(\frac{t-t_c^{(2)}}{\sigma_c^{(2)}}\right)^2} \tag{10}$$

The reason for including a time offset t_c is that the true amplification is only Gaussian in approximation. Since we are only observing events at $t > 0$, there is no need to keep $\mathcal{F}(t)$ symmetric and an offset can be introduced to improve the description of the data. The addition of the second gaussian is believed to be prompted by the fact that individual beam bunches start to overlap.

A point of special interest is pileup with invisible pulses. It is believed that the main problem of the first version of MilliFitter (*i.e.* one in which the error-bars where scaled with the energy), was that the average effect of small pulses was to increase the energy of larger pulses. Moreover, the amount of increase was proportional to the length of the island, which by itself was related to time[5].

3.3 Coherent Betatron Oscillations

The effect of betatron oscillation on the measurement of $(g-2)$ has been described by Yuri[6]. The most prominent effect is the modulation of positron rate on the calorimeters. Due to the breathing of the beam and the movement of the (average) geometrical location of the beam, the "cone" of positrons hitting the face of the detector will be cut off because of the limited (mainly vertical) acceptance of the vacuum chamber and it inhabitants. Moreover, the acceptance of the calorimeter does not cover this cone completely, so when the cone widens or moves, a different part of the cone will be probed, with a possibly different intensity. So, coherent betatron oscillations will lead to a modulation of the rate. In other words, it is a multiplicative effect, which has to be taken into account *squared* for the pileup events. The most important result of this is the *doubling* of the modulation amplitude compared to that for the single events.

It has not been firmly established whether the modulation amplitude depends on the positron energy. If the latter were the case, this would lead to a serious complication for

the rate modulation of the pileup events. For the moment, it is assumed that there is no energy dependence and that the rate is simply modulated as,

$$C(t) = 1 + e^{-\frac{1}{2}\left(\frac{t-t_\beta}{\sigma_\beta}\right)^2}\left[\hat{A}_c \cos\omega_\beta t + \hat{A}_s \sin\omega_\beta t\right]. \tag{11}$$

The five parameters used to parametrize the rate modulation are the frequency and phase, the modulation amplitude, coherence time and time offset. Of these parameters, the phase and the modulation amplitude are free floating during the fit because they differ per detector and perhaps as a function of the positron energy, *viz.* via the applied energy cut. The other parameters are believed to be common to all detectors, since they represent a property of the muon beam itself and not its decay products. They are therefore determined from independent analyses. The asymmetry and phase of the CBO signal can be obtained in a similar way as the $(g-2)$ asymmetry and phase (see eqs. (5)–(8); use $N = 1$ and $dN = 0$).

3.4 *Energy Scale Changes*

Instead of correcting the energy scale on an event-by-event basis, the correction for changes in the energy scale was done in the fitting function. For small enough changes, the problem can be linearized, as shown in the expressions below.

$$\begin{aligned}\frac{N(g;E_1,E_2)-N(1;E_1,E_2)}{N(1;E_1,E_2)} &= \frac{\int_{E_1/g}^{E_2/g}\mathcal{N}(E)dE - \int_{E_1}^{E_2}\mathcal{N}(E)dE}{\int_{E_1}^{E_2}\mathcal{N}(E)dE} \approx (g-1)\left(\frac{\int_{E_1}^{E_2}\frac{d\mathcal{N}}{dE}EdE}{\int_{E_1}^{E_2}\mathcal{N}(E)dE}+1\right) \\ &\equiv \frac{dN}{d\mathcal{G}}(g-1)\end{aligned} \tag{12}$$

When substituting $\mathcal{N}(E)$ with $\mathcal{N}(E)A(E)$, the effect on the amplitude of the $(g-2)$ wiggle can be calculated. The issue of a phase shift is more complicated, but what it boils down to is that there is a phase-shift which is proportional to the change in the gain, with a proportionality constant which depends on the energy range. Because the effect of an energy scale change is small by itself, it is only applied on the nominal part of the wiggle function. The change in N, NA and the phase shift $\Delta\phi$ are calculated as

$$N(t) = N_0 + \frac{dN}{d\mathcal{G}}\Delta\mathcal{G}(t) \tag{13}$$

$$NA(t) = NA_0 + \frac{dNA}{d\mathcal{G}}\Delta\mathcal{G}(t) \tag{14}$$

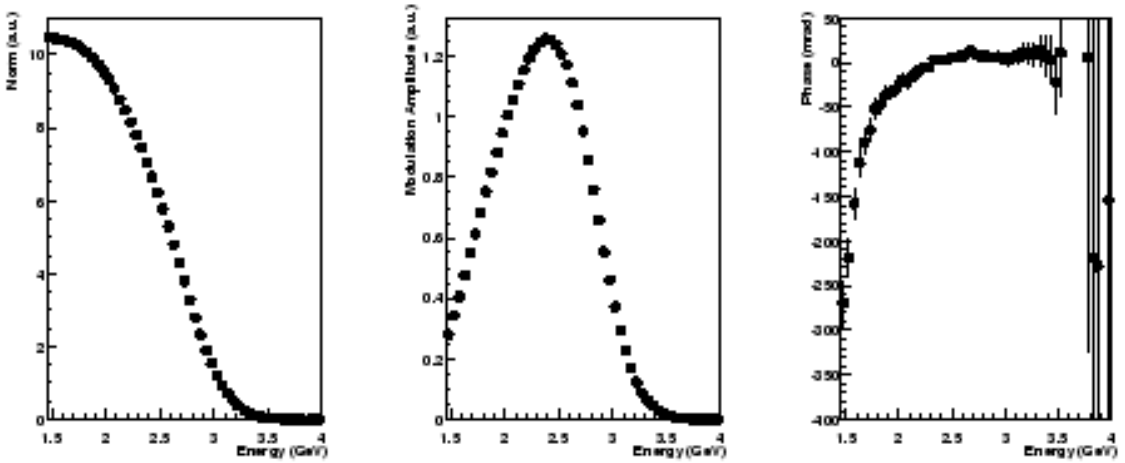

Figure 1. Energy dependence of N, NA and ϕ (for detector 19).

$$\Delta\phi(t) = \frac{d\phi}{d\mathcal{G}}\Delta\mathcal{G}(t) \tag{15}$$

The sensitivities to energy scale changes are given in table 13. These parameters were obtained from the data itself by Fourier-transforming a pileup-subtracted time spectrum for narrow energy bins. The values for $\frac{dN}{d\mathcal{G}}$ and $\frac{dNA}{d\mathcal{G}}$ were derived from the energy dependence of the amplitude at $f = 0$ and $f = 229.1$ kHz, respectively. The value of $\frac{d\phi}{d\mathcal{G}}$ was obtained from the energy dependence of the phase, weighted with the modulation amplitude (see fig. 1). A complication here is that the sign of this sensitivity depends on the parameterization of the $(g-2)$ wiggle as used in the fit.

The time dependence of the energy scale change (ESC) is parameterized as

$$\Delta\mathcal{G}(t) = N_1 e^{-t/\tau_1} + N_2 e^{-t/\tau_2} \tag{16}$$

The value for N_1, τ_1, N_2 and τ_2 were extracted from a fit to the average energy histograms after correcting for the contribution of pileup (see table 12).

A study (see figs. 13 – 16) showed that the average energy changes with time and can be described by the function

$$\hat{E} = \hat{E}_0\left[1 + \epsilon\Delta\mathcal{G}(t)\right] = \hat{E}_0\left[1 + \epsilon\left(N_1 e^{-t/\tau_1} + N_2 e^{-t/\tau_2}\right)\right] \tag{17}$$

Here, ϵ accounts for the sensitivity of a change in the average energy given a change in the gain. For $E > 2$ GeV, $\epsilon \simeq \frac{1}{2}$. The results for all detectors can be found in tab. 12. The

values for τ_1 range from 15 to 50 μs, which is close to the typical time scale of muon loss and pileup.

A significant difference between the first and second version of MilliFitter is obvious from the time dependence of the average energy, which is believed to be due to the influence of the invisible pulses (so *not* a mistake in the fitter itself). In the first version, this influence on the energy was not canceled, whereas the second version was setup to do precisely that.

As part of the study of the time dependence of the average energy, the earliest times at which the behaviour seems reasonable was established (see tab. 12). Only detector 1 has an obvious problem. The bump observed at very early time originates from tube 1. Applying a global energy scale correction will induce a disturbance of the data. As long as the origin of this bump and other similar peculiarities in the average energy are not resolved, data before the occurance of this event are not used. Consequently, also the data for all detectors combined shouldn't be used before this time. For all other detectors no obvious problems are observed. Further, it should be noted that the gain changes are very small and that correcting for them is unnecessary. As a matter of completeness, however, a (very small) gain correction is applied.

3.5 *Muon Losses*

The loss of muons other than by decay leads to a change in the positron rate on the calorimeters, *i.e.* it is a multiplicative term. For the pileup part, this term has to be squared of course. The functional form follows from the differential equation

$$\frac{dN}{dt} = -\frac{1}{\tau}N - \beta(t)N = -\frac{1}{\tau}\left(1+\beta'(t)\right)N \tag{18}$$

with $\beta(t)$ the absolute loss rate as a function of time and $\beta'(t)$ the fractional loss per lifetime. Dave found that $\beta(t)$ can be described to acceptable precision with an exponential time dependence, $\beta(t) = A_\Lambda\, e^{-t/\tau_\Lambda}$, which leads to

$$N(t) = e^{-\frac{1}{\tau}\left(t + A_\Lambda \tau_\Lambda\left[1-e^{-t/\tau_\Lambda}\right]\right)} = e^{-\frac{t}{\tau}} \times e^{\frac{A_\Lambda \tau_\Lambda}{\tau}\left[1-e^{-t/\tau_\Lambda}\right]} \tag{19}$$

Time independent muon loss is not considered here, because it will be absorbed in the lifetime and lower it by some fixed amount.

Table 2
List of tunable and fitted parameters.

Variable name	symbol	description
1/lifetime	k	inverse of the lifetime
N	N	normalization of the nominal component
NAcosphi	A_c	amplitude of the cosine $(g-2)$ term
NAsinphi	A_s	amplitude of the sine $(g-2)$ term
R	R	deviation of f_a from 229.1 kHz in ppm
PuNorm*	N_2	normalization of the pileup component
PuNA1*	A_p	amplitude of the 1^{st} harmonic pileup term
PuPhi1†	$\Delta\phi_1$	phase shift of 1^{st} harmonic pileup term
PuNA2*	A_{p2}	amplitude of 2^{nd} harmonic pileup term
PuPhi2†	$\Delta\phi_2$	phase shift of the 2^{nd} harmonic pileup term
FFNorm†	A_ϵ	amplitude of pileup enhancement due to fast rotation
FFLifetime†	σ_ϵ	coherence time of the PU enhancement envelope
FFTimeOffset†	t_ϵ	time offset for PU enhancement envelope
FFNorm2†	$A_\epsilon^{(2)}$	2^{nd} amplitude of pileup enhancement due to fast rotation
FFLifetime2†	$\sigma_\epsilon^{(2)}$	2^{nd} coherence time of the PU enhancement envelope
FFTimeOffset2†	$t_\epsilon^{(2)}$	2^{nd} time offset for PU enhancement envelope
CBOFrequency†	ω_β	frequency of the coherent betatron modulation
CBOLifetime†	σ_β	coherence time of the CBO modulation envelope
CBOTimeOffset†	t_β	time offset for CBO evelope
CBOAcosphi	$\hat{A}_c$	amplitude of the cosine term of the CBO modulation
CBOAsinphi	$\hat{A}_s$	amplitude of the sine term of the CBO modulation
MuLossNorm‡	A_Λ	time dependent muon loss per lifetime
MuLossLifetime†	τ_Λ	extinction rate of time dependent muon loss
GSN1†	N_1	first amplitude to describe time dependent ESC
GSTau1†	τ_1	decay time of first TDESC
GSN2†	N_2	second amplitude of TDESC
GSTau2†	τ_2	decay time of second TDESC
dNdGS†	$\frac{dN}{dG}$	change in N for a changing gain
dNAdGS†	$\frac{dNA}{dG}$	change in NA for a changing gain
dPhidGS†	$\frac{d\phi}{dG}$	phase-shift for a changing gain

* zero for pileup subtracted spectra
† always fixed
‡ fixed when pileup if fitted

3.6 *Summary*

A list of all variables and their meaning is given in table 2.

4 Results

In this section, the methods and results for finding the fixed parameters are described and results for the floating fit parameters are discussed.

Assuming that the functional form is adequate to describe the data, averaging the fitting results per detector and fitting the sum of the detectors must yield identical results. Furthermore, fitting the detectors individuallly opens the possibility to average the results for different start times so that phase pulling effects can be reduced. Furthermore, by fitting the detectors individually, the distribution of χ^2, and thus the accuracy of the model is probed in more detail than when just the sum is fitted. Also, we know that two of the detectors (1 and 4) have problems at early times, which prevents fitting the sum of all detectors without assigning an additional systematic error.

An argument for fitting the detectors together is that effects such as that caused by the coherent betatron oscillation tend to have different phases for different detectors. Since they are added coherently, the overall amplitude of oscillatory phenomena will decrease. Furthermore, the magnitude and time dependence of the individual energy scale corrections are mostly statistical in nature, so that when added together the overal correction becomes smaller.

A hybrid approach was tried in which the "clean" detectors were added together before being fitted and detectors 1 and 4 were fitted individually. The fitting results were then averaged to obtain the maximal statistical accuracy.

It has been demonstrated in the analysis of the 1998 data, that minimizing $\sum \chi_i^2$ with $\chi_i^2 = \left(\frac{N_i - f(t_i)}{\sqrt{N_i}}\right)^2$ leads to a biased result. The correct result is obtained when $\left(\frac{N_i - f(t_i)}{\sqrt{f(t_i)}}\right)^2$ is used instead. Cenap and Alex establish this by iterating. In the first iteration, χ_i^2 is calculated based on $\sqrt{N}$. For the next iterations, the errors are substituted by $\sqrt{f}$, with f from the previous fit. In this analysis, χ^2 is directly calculated as $\sum_i \left(\frac{N_i - f(t_i)}{\sqrt{f(t_i)}}\right)^2$, so that iteration can be avoided.

4.1 Fixed Parameters

Because the function described in the previous section has too many parameters to be fit directly, most of them were kept fixed. In general, the change in a (carefully chosen) fitting parameter for two different fits is compared to the allowed change based on the overlap of the data for those two fits. The parameters to be optimized were varied using a binary search method until the change in the fitting parameter was less than 10% of the

allowed variation. This method is expected to be consistent with minimumizing χ^2. The final systematic errors are derived from manually minimizing χ^2.

The two methods complement each other in the sense that the first method focusses on global stability of the optimized parameter. A χ^2-minimization yields a locally best value.

Below is described how the values for specific parameters were obtained. In summary,

- pileup enhancement terms are obtained from the fast rotation histogram;
- pileup-to-normal phase difference is obtained from the requirement that the $(g-2)$ phase is independent of the amount of pileup; actual values were taken from a pileup simulation after statistical agreement between the experimental values and this model was found.
- the coherent betatron frequency $\omega_\beta = 2\pi \times (470.433 \pm 0.014)$ kHz is obtained from the requirement that the CBO phase is independent of start time. The χ^2 minimization yielded $\omega_\beta = 2\pi \times (470.416 \pm 0.033)$ kHz, leading to a systematic error in R of 4×10^{-4} ppm.
- the coherent betatron coherence time $\sigma_\beta = 124$ μs, and time offset $t_\beta = -30$ μs are obtained from the requirement that the CBO asymmetry is independent of start time. The χ^2 minimization gave $t_\beta = 108.3 \pm 1.4$ μs, with a systematic error in R of 3×10^{-3} ppm.
- the muon loss time $\tau_\Lambda = 27.46$ μs is obtained from Daves FSD coincidence studies; A χ^2 minimization yielded a value of 31.2 ± 1.1 μs (for the average over 22 detectors) and a systematic error of 1.3×10^{-3} ppm.
- the muon loss amplitude A_Λ is obtained from the requirement that the pileup normalization is twice as big for a $\Delta t = 10$ ns data set as for a $\Delta t = 5$ ns data set.

4.1.1 *Pileup Related Parameters*

Although the preferred result of this analysis is obtained from a pileup corrected data set, the methods and results to derive the pileup amplification due to the fast rotation and the pileup are explained below.

Pileup Amplification due to Fast Rotation

The most easily obtained parameters are those related to the amplification of the pileup due to the fast rotation. For each detector a histogram of the events with an energy between 1 and 1.2 GeV was made. For this energy, there is no $(g-2)$ modulation. The bin-width of these histograms was taken to be 5 ns, which corresponds to the minimum deadtime used in this analysis. This histogram clearly shows the modulation of the rate due to the fast rotation. The next step is to construct the ratio $\frac{\langle R^2 \rangle}{\langle R \rangle^2}$ from these data. This is done by adding the events in 29 consecutive bins ($\equiv 29 \times \langle R \rangle$) and adding them after

squaring ($\equiv 29 \times \langle R^2 \rangle$). The resulting histogram can then be fitted. The average fit values are $A_\epsilon = 1.272$, $t_\epsilon = -4.224\ \mu$s and $\sigma_\epsilon = 13.52\ \mu$s for the first bump and $A_\epsilon^{(2)} = 2.974 \times 10^{-3}$, $t_\epsilon^{(2)} = 53.14\ \mu$s and $\sigma_\epsilon^{(2)} = 7.854\ \mu$s.

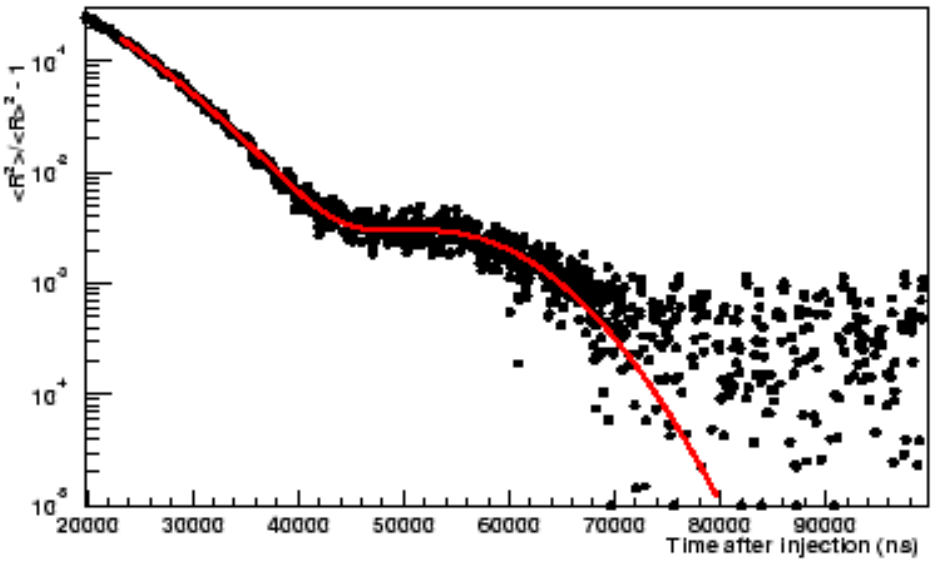

Figure 2. Ratio between average square of the rate and square of the average rate as a function of time after injection and the sum of two gaussians fitted to this ratio.

The amplitude σ_ϵ can be estimated from the width of the injected beam bunch. For a gaussian beam profile, the pileup amplification will be $T/\left(2\sqrt{\pi}\sigma\right)$, which for $T = 149.14$ ns and $\sigma = 25$ ns leads to an amplification of $\sigma_\epsilon = 0.68$ at injection. The observed value of 0.952 at $t = 0$ can be obtained for $\sigma = 23$ ns, which is entirely reasonable. The width σ_ϵ is related to the width of the Fourier-transform of the fast rotation data, which has an RMS of 16 kHz. Assuming a Gaussian frequency spectrum, this would lead to $\sigma_\epsilon = 14.1\ \mu$s, which is suffiently close. Finally, the offset t_ϵ accounts for the fact that the frequency spectrum is not perfectly Gaussian. The observed offset of about 1 μs is probably small enough to be reasonable.

Phase Difference between Normal and Pileup Wiggle

The most important pileup parameter to fix is the phase of the first harmonic, because it increases the fitting error on ω by a factor two. The procedure used to experimentally determine this phase is by eliminating the difference in the fitted $(g-2)$ phase for deadtimes of 5 and 10 ns.

The experimental values that were found using the first version of Millifitter are in rea-

Table 3
Phase difference between normal and pileup wiggles for various energy ranges. The "average" value was extracted by averaging the results obtained for individual detectors. The result marked "sum" is for the sum of all detectors.

Energy range (GeV)	$\Delta\phi$ (mrad)		
	Geant	average	sum
1.8 – 3.1	1.6	1.4±1.7	0.8±1.6
1.8 – 6.2	28.8	8.4±6.9	34.4±13.3
2.0 – 3.1	1.9	12.9±1.2	4.7±5.6
2.0 – 6.2	-16.2	15±83	-75±30

sonable agreement with those predicted using the Geant results (see table 3). The latter has an unknown, but presumably sizeable uncertainty as well. In the actual fitting, the (independent) results obtained from Geant are used. Furthermore, in determining these phase differences from the data, the correlation with ω and the phase of the normal part of the wiggle may lead to biased results. It is therefore deemed safer to use the Geant results.

4.1.2 *CBO Related Parameters*

The CBO related parameters must be extracted from a pileup free data sample. The reason for this is the possibility of very strong interference between the second harmonics of the pileup, which has a frequency of about 454 kHz and the CBO signal, which has an expected frequency of $\left(1-\sqrt{1-n}\right) f_c \simeq 470$ kHz ($f_c \simeq 6.7$ MHz is the cyclotron frequency and $n \simeq 0.135$ the weak focussing field index).

The CBO frequency ω_β was found by eliminating the difference in the CBO phase fitted at t_{start} and t_{start}+50 μs after injection. When there is a small frequency mismatch, this will manifest itself as a slow change in the phase. For $E > 2$ GeV, the average of the frequencies found for individual detectors is 470.41 kHz with an error of about 14 Hz. For all detectors combined, a frequency of 470.66 kHz is found, with an error of 90 Hz.

The CBO lifetime σ_β was determined by requiring that the CBO modulation amplitude is independent of the start time of the fit. An average value of $\sigma_\beta = 88.5$ μs was found when all detectors were fitted separately. The sum of the detectors yielded a value of 92.9 μs with an error of 2.3 μs.

The expected value is about $1/\sqrt{2}\left(1-\sqrt{1-n}\right) = 10$ times larger than the extinction time of the fast rotation (the factor $\sqrt{2}$ comes from the fact that the rate is squared to extract σ_ϵ). The extinction time σ_ϵ of the pileup amplification was found to be 13.62 μs, so that $\sigma_\beta \simeq 136$ μs. The values found are more of the order of 90 μs, but more important, they depend on the start time of the optimization routine (see table 4).

Table 4
CBO lifetime for station 17 with $t_\beta = 0$.

t_{start} (μs)	τ_β (μs)
22.8	82.0 ± 2.4
32.8	92.7 ± 3.5
42.8	102.7 ± 4.7
52.8	111.3 ± 6.0
62.8	115.9 ± 8.0
72.8	119.1 ± 8.6

The are a few explanations for this time dependence. First, it can indicate that the parameterization is not optimal and that a time offset such as used for the parameterization of the pileup enhancement term might improve the description. The time dependence of τ_β in table 4 can be fitted to the function $\tau_\beta(t_{start}) = \frac{\tau_\beta t_{start}}{t_{start}-t_\beta}$ to yield $\tau_\beta = 149 \pm 12\mu$s and $t_\beta = -18.5 \pm 3.9\mu$s.

The systematic error estimate was based on χ^2 minimization. This was done by scanning the CBO frequency over different values, perform a normal fit for each individual detector at the earliest start times and then add the χ^2. In fig. 3 the summed χ^2 and the average R are shown for a single randomization sequence. The fit shown in red is $\chi^2(f) = \left(\frac{f-f_0}{\sigma_f}\right)^2 + \chi_0^2$ and yields $f_0 = 470.416 \pm 0.033$ kHz. The same functional form was used to fit the dependence of R on ω_β, which is obviously extremely small, leading to a systematic error of less than a part-per-billion. The optimal value for a specific set of start times might not

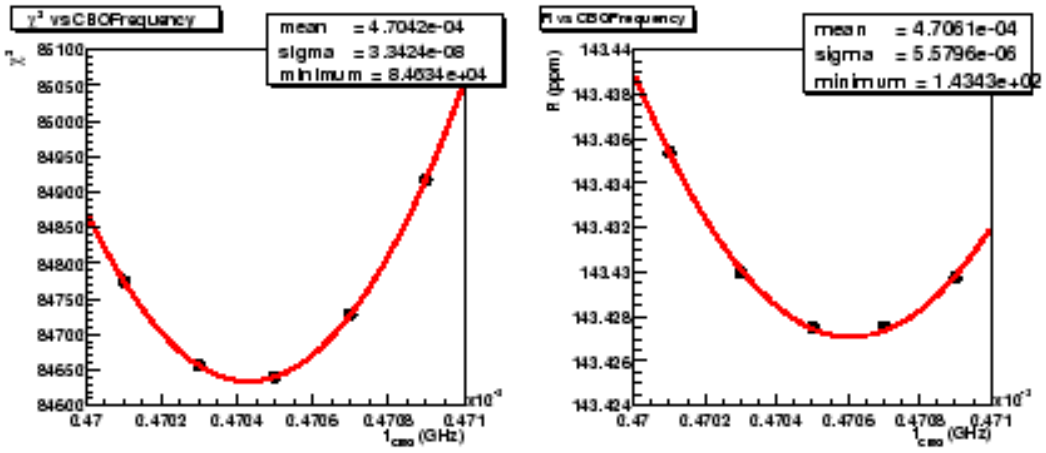

Figure 3. Sum of the fitting χ^2 (top) and average R for all 22 detectors as a function of the CBO frequency. The number of degrees of freedom is 82826. The start times for the individual detectors are the same as those used to obtain the average value for R. Note that a single randomization sequence was used.

be optimal for other start times, which may be reflected by a start time dependence of the

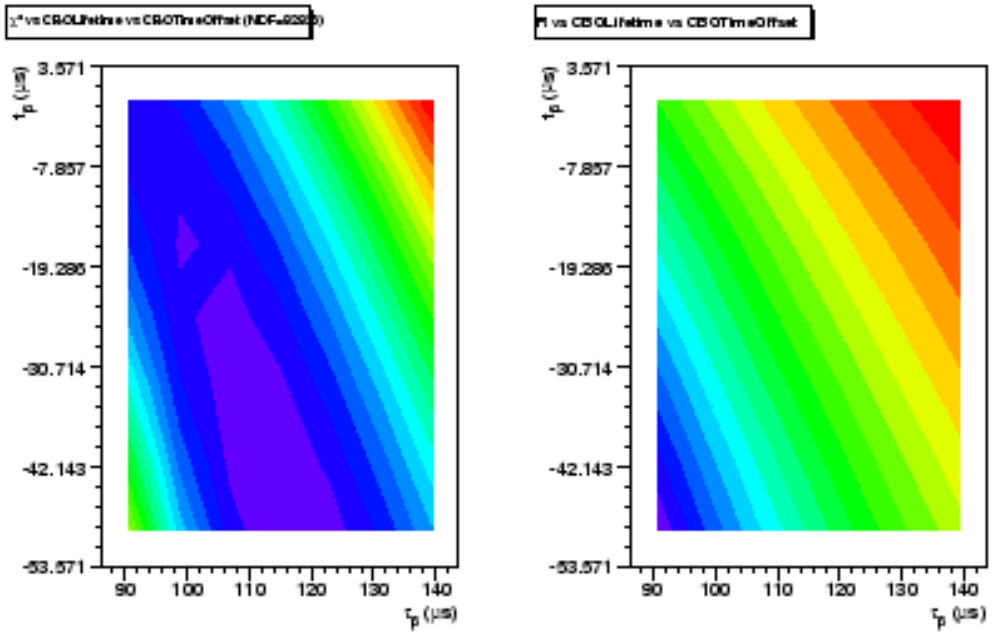

Figure 4. Sum of the fitting χ^2 (left) and average R for all 22 detectors as a function of the CBO time constants. The start times for the individual detectors are the same as those used to obtain the average value for R. Note that a single randomization sequence was used. The contour levels are 37 and 0.007 ppm for χ^2 and R, respectively.

CBO phase.

The previously observed correlation between τ_β and t_β is obvious when a χ^2 minimization is done (see fig. 4). The location of the minimum in χ^2 for a fixed value of the time offset is shown in fig. 5, which shows the strong dependence. The values used in the fits described below were $\tau_\beta = 108\ \mu$s and $t_\beta = -30\ \mu$s. This choice leads to an increase of the χ^2 by 0.0001, a shift in R of -0.002 ppm and an uncertainty of 0.003 ppm.

4.1.3 Muon Loss Related Parameters

David Hertzog studied the lost muons with FSD coincidences. From his studies, a muon loss timescale $\tau_\Lambda = 27.460\ \mu$s was derived, but with a strong sensitivity to the start time of the fit.

Trying to fit the data while floating both the muon loss amplitude and timescale prohibited convergence within a reasonable number of iterations. The timescale was therefore fixed for most of the fits. The amplitude on the other hand could be floated when fitting data sets that were corrected for pileup. Only when fitting the sum of the detectors at early start times (so increase statistical precision), both were floated at the same time.

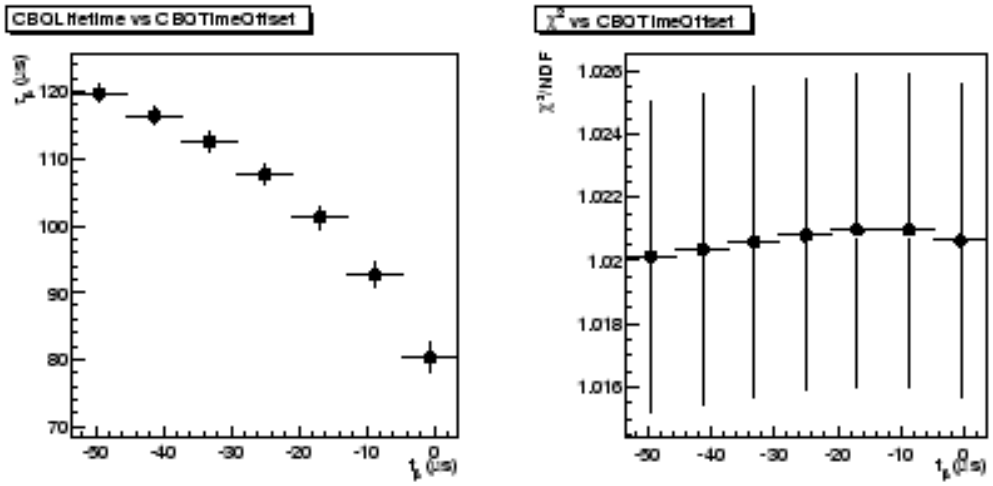

Figure 5. Value of τ_β for a fixed value of t_β and the minimum reduced χ^2.

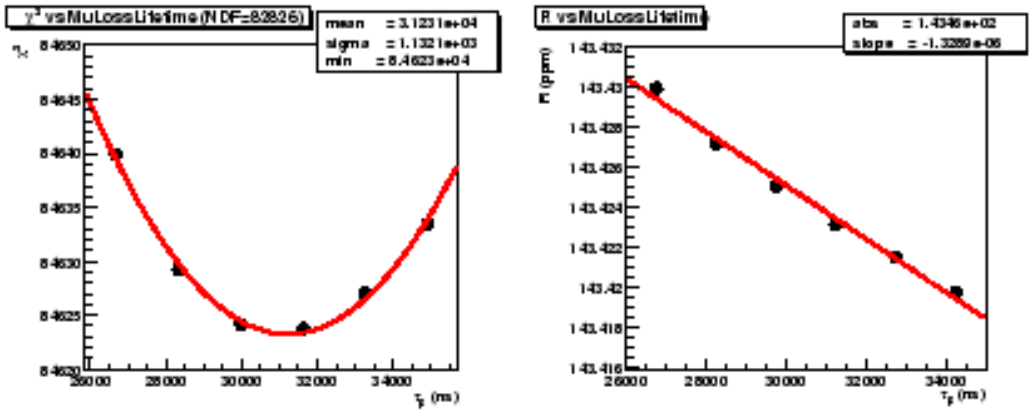

Figure 6. Value of χ^2 and R as a function of τ_β, summed and averged over the detectors, respectively.

The strong correlation between the pileup amplitudes and the muon loss fraction A_Λ was exploited to determine the latter. Two data sets with a deadtime of 5 and 10 ns are both fitted to a function with the pileup amplitudes floating and the muon loss fraction fixed. With the assumption that the amount of pileup is proportional to the deadtime, the muon loss fraction can be varied until the ratio between the pileup normalization constants for both deadtimes is 2. To get the biggest sensitivity, this optimization is done for a start time as small as possible.

A χ^2 minimization at the earliest start times yielded a optimal lifetime of 31.2 ± 1.1 μs (see fig. 6). The corresponding systematic error in R is 1.7×10^{-3} ppm.

The fitted value for the "clean" sum of detectors at about 32 μs was 22.0 ± 1.1 μs with a

Table 5
Values of the fixed parameters used in this analysis.

CBOFrequency	ω_β	470.43 kHz
CBOLifetime	σ_β	108.313 μs
CBOTimeOffset	t_β	-30 μs
MuLossLifetime†	τ_Λ	31.129 μs

† floated for sum

considerable reduction in the χ^2 (1.007 vs. 1.027). The origin of this stricking discrepancy with the result obtained when averaging the detectors is not known at this point. From the sensitivity of R to τ_β derived above, this leads could lead to a systematic shift of 0.012 ppm, which is therefore included in the systematic error.

4.2 *Floating Parameters*

In general little more than a handfull of parameters were floated. These parameters of course include the usual five parameters. Because the data were corrected for pileup, the pileup related amplitudes were kept at zero and the muon loss fraction was floating instead. Since the CBO modulation amplitude and phase may vary by detector, they are also kept floating. All the other parameters had fixed values. For the "clean" and full sum, the muon loss lifetime was floated as well. The values of the fixed parameters can be found in table 5. The corrections for the varying energy scale are detector dependent and can be found in table 13.

4.2.1 *Magnitude and Stability of χ^2*

The consistency of the χ^2 with its expected value and its stability as a function of the start time are the first requirements for a believable fit. The results in fig. 7 show that only the fits for detector 1 and 4 are obviously poor before 30 μs. The χ^2 of detector 1 steeply rises to unacceptable values at start times before 40 mus. The one of detector 4 doesn't seem to settle at a stable value untill 100 μs after injection. The χ^2's for the other detectors are all stable from 30 μs on; most of them are stable as early as 25 μs. The χ^2 for the sum of all detectors is acceptable (within 1σ of 1) from about 36 μs on, whereas that of the "clean" sum (all but 1 and 4), is consistent with 1 from about 28 μs.

A direct comparison between the fitted values of R obtained from fitting the sum of the detectors and from fitting individual detectors is shown in fig. 8. The difference between the result for the sum and the average of the results for the individual detectors is modulated with the $(g-2)$ frequency with a 0.28 ppm amplitude peak-to-peak at 30 μs. At 100 μs, this has gone down to 0.13 ppm peak-to-peak. The difference between the result for the full sum and that obtained from averaging the "clean" sum and the result for de-

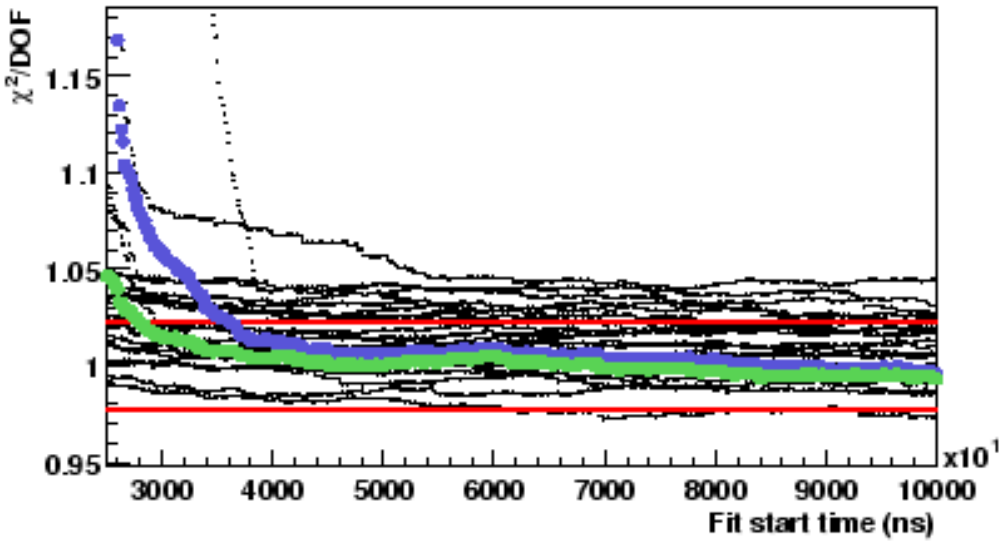

Figure 7. Dependence of random sequence averaged χ^2 per degree of freedom for all 22 detectors. The 1σ level is indicated with the red lines. In blue, the result for the sum of all 22 detectors is shown and in green that for the sum except 1 and 4.

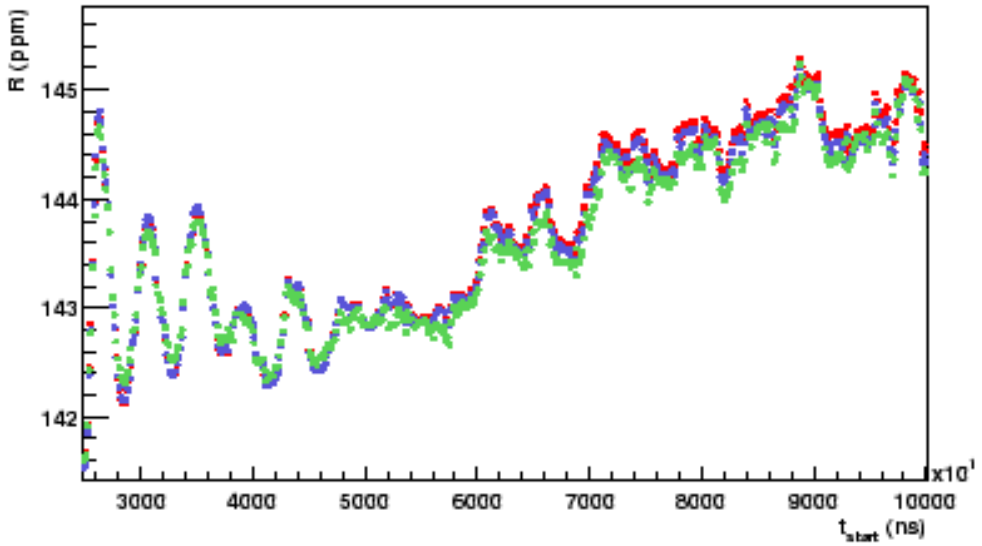

Figure 8. Start time dependence of R on the fitting method. The result obtained from fitting the sum of all detectors is shown in red, that from averaging the fits to the "clean" sum and 1 and 4 independently in blue, and that from averaging the fits to all individual detectors in green.

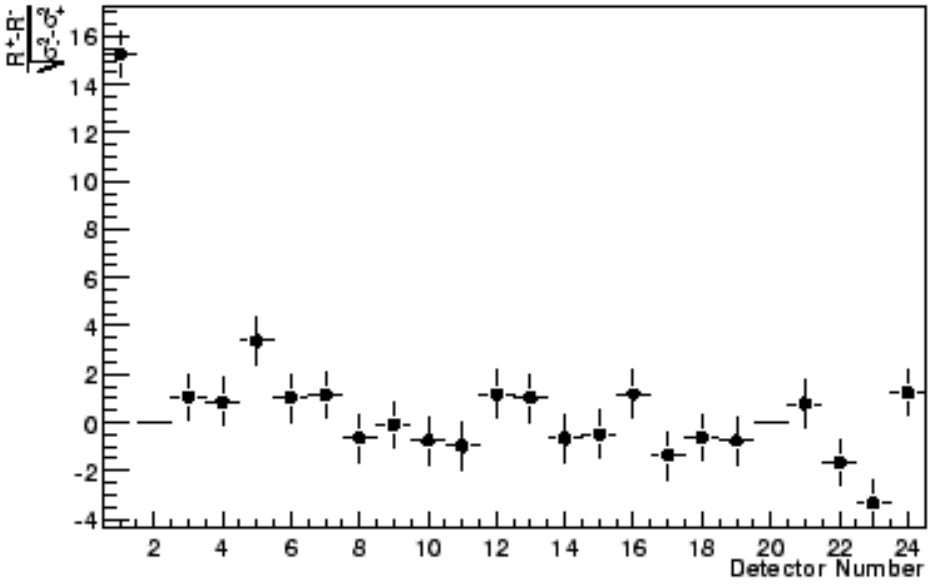

Figure 9. Difference in R for t_{start} = 31.649 ±0.5 μs in units of $\sqrt{\sigma_1^2 - \sigma_2^2}$.

tectors 1 and 4 is modulated at both the $(g-2)$ and CBO frequency, with a peak-to-peak amplitude of 0.04 ppm at 30 μs. A slowly increasing difference of 0.1 ppm is seen between 30 and 100 μs.

The most important observation at this point us that R shows a considerable amount of phase pulling at early times. In fig. 9, the amount of phase pulling at 31.6 μs is shown. This amount is obtained by taking the difference in R on the peak and trough just before and after 31.6 μs. Clearly, detector 1 stands out. Including detector 1, the average is 0.76 ± 0.21; excluding 1 lowers this to 0.07 ± 0.22.

4.2.2 *Start Time Stability*

The next step is to investigate the stability of the other parameters as a function of start time. The results for individual detectors as well as those for the full and "clean" sum can be found in figs. 17–40. From top to bottom and from left to right, these plots show: (χ^2/NDF , R , N), (A_c , A_s , k) and (A_Λ , $\hat{A}_c$ and $\hat{A}_s$), all versus fit start time measured in ns since injection.

In the plot showing the time dependence of R, the expected deviations are indicates by the size-ways parabola, which is based on the old Kawall formula. For each detector, the tip of the parabola starts at the time at which the final result is obtained (see table 6). These start

Table 6
Start times used to obtain the final result

t_{start} (μs)	25.101	27.284	29.467	31.649	33.832	36.015	49.111	55.659
det	12, 16–18, 22–24	9, 14	7, 10, 11, 13, 15	5,6,8	19	3	1	4

Table 7
Average parameter correlation coeficients matrix at the start times from table 6.

	k	N	A_c	A_Λ	R	A_s	$\hat{A}_s$	$\hat{A}_c$
k	1.000	-0.635	-0.602	-0.744	-0.004	-0.005	-0.002	0.010
N	-0.635	1.000	0.948	0.984	0.001	0.003	0.005	-0.018
A_c	-0.602	0.948	1.000	0.932	0.001	0.002	0.005	-0.018
A_Λ	-0.744	0.984	0.932	1.000	0.001	0.003	0.005	-0.017
R	-0.004	0.001	0.001	0.001	1.000	0.825	0.002	-0.001
A_s	-0.005	0.003	0.002	0.003	0.825	1.000	0.002	0.000
$\hat{A}_c$	0.010	-0.018	-0.018	-0.017	-0.001	0.000	-0.006	1.000
$\hat{A}_s$	-0.002	0.005	0.005	0.005	0.002	0.002	1.000	-0.006

times are all chosen to correspond to $(g-2)$ zero crossings, where even in the presence of phase-pulling, the fit results for R are believed to reflect to "true" value. Further reasons to pick a certain start time were the value and stability of the χ^2 and the stability of R. What further guided the choice of these start times was the overall parameter stability for other data sets as well, notably the energy range 1.8 – 3.1 GeV without pileup subtraction.

At first sight, the stability of R (and hence A_s) looks acceptable, whereas that of all the "normalizing" parameters (N, A_c , k, A_Λ) is rather poor. However, all 4 seem to exhibit the same trend, which indicates a strong correlation. Table 7 contains the parameter correlation coefficient matrix averaged over the individual detectors for fits at their respective start times. As expected, there is a strong correlation between R and A_s. Because the time offset were adjusted, the latter is essentially the phase. Also obvious is the essentially complete correlation between k, N, A_c and A_Λ. So what we see is probably an exhibit of a strong correlation with an poorly determined parameter, because out of these four parameters, only A_Λ is expected to have a large uncertainty. Assuming two parameter correlation only, the expression for χ^2 is

$$\chi^2 = \chi^2_{min} + \sum_i \left(\frac{\Delta x_i}{\sigma_{x_i}}\right)^2 + \sum_{j>i} 2a_{ij}\frac{\Delta x_i}{\sigma_{x_i}}\frac{\Delta x_j}{\sigma_{x_j}}. \tag{20}$$

Obviously, when $a_{ij} = 1$ for some pair (i, j),

$$\chi^2 = \chi^2_{min} + \left(\frac{\Delta x_i}{\sigma_{x_i}} + \frac{\Delta x_j}{\sigma_{x_j}}\right)^2 + \cdots \tag{21}$$

So for completely correlated variables, $\Delta x_i = \frac{\sigma_{x_i}}{\sigma_{x_j}} \Delta x_j$ will all give the same χ^2. Because the values of the fixed parameters were optimized to give the lowest possible χ^2 at the start times used to obtain the final result, these values may not be optimal to assure start time stability, which is what is observed.

When the value of A_Λ is adjusted to its value at time for which the fixed parameters were optimized and the change in the other parameters is calculated as $Dx_i = a_{i\,A_\Lambda} \frac{\sigma_{x_i}}{\sigma_{A_\Lambda}} DA_\Lambda$, and $D\chi^2 = \sum_i 2a_{i\,A_\Lambda}(a_{i\,A_\Lambda} - 1)\left(\frac{\Delta A_\Lambda}{\sigma_{A_\Lambda}}\right)^2$. The effect of this adjustment shown in fig. 41 for the "clean" sum. Similar trends are seen for individual detectors and the full sum. Note that the uncertainties were not adjusted and that the parameter correlation coefficients from table 7 were used at all start times.

After this adjustment the stability of the parameters is excellent. The observed time dependence can almost entirely by accounted for assuming a drift in the muon loss fraction A_λ, which is poorly determined, strongly correlated to the muon loss lifetime τ_Λ which was fixed and strongly correlated to many other parameters. Note that neither χ^2 nor R have changed notably.

4.2.3 *Residuals at Final Start Times*

To check for components in the data that the fitting function did not account for, the fitting residuals were Fourier transformed. Since the detectors have different fit start times, the residuals were normalized to $Ne^{-kt_{start}}$. The Fourier transformation interval was the same for all detectors and extended from the fit start time till 2048 bins later (307.2 μs).

By averaging the amplitude spectra for the individual detectors, the magnitude of an unaccounted contribution can be obtained and compared to the average background level (see fig. 10). One can also determine the amplitude of the average of the complex Fourier spectra. In that case, the noise level will be reduced by $\sqrt{22}$ so that also smaller peaks can be observed. On the other hand, signals that are out of phase in the individual detectors will show a reduced amplitude when this procedure is employed.

Obvious peaks are the ones at 1.7 MHz (vertical CBO envelope modulation; *a.k.a.* vertical waist) and 2.25 MHz (flashlets). There is a possible peak near 940 KHz (second CBO harmonic), although very faint. The vertical waist peak can be fitted to a gaussian with a peak position of 1.72 MHz and a width of 22.6 kHz. This describes a signal in the time domain with a Gaussian width of about 7 μs (or approximately 9.3 μs if the muon lifetime if folded out). Table 8 lists the approximate contributions of individual detectors.

The negative spike near 470 kHz has the right location and width to signal a small CBO remnant. This remnant is in anti-phase with the main contribution to that frequency and

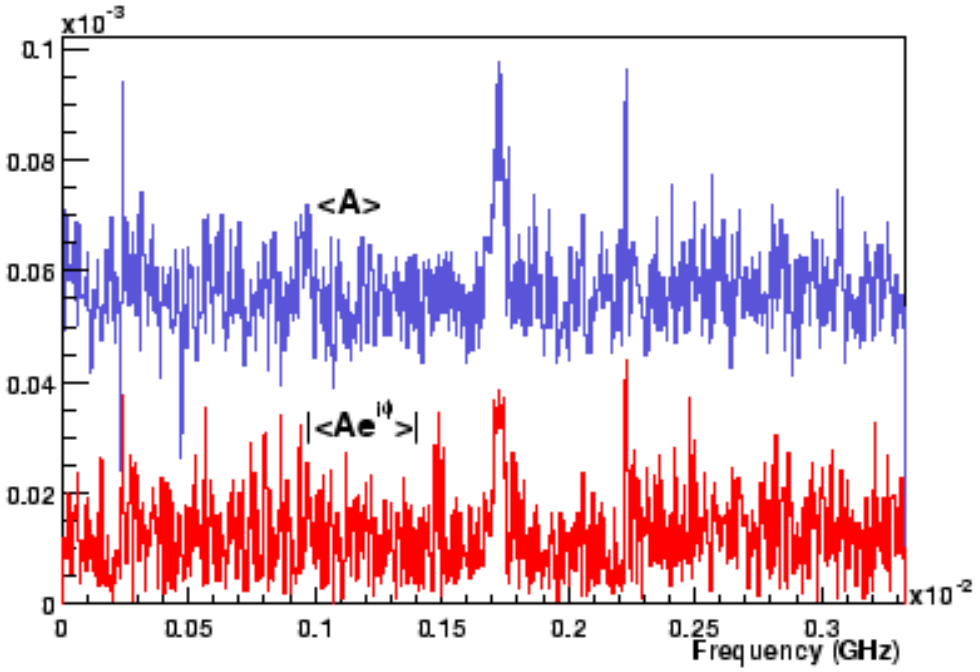

Figure 10. Average normalized Fourier amplitude spectrum for a single randomization seed. In blue (top) the average Fourier amplitudes; in red the amplitude of the average complex Fourier spectrum.

Table 8
Contributions to the average vertical waist peak for individual detectors. Unlisted detectors could not be fitted

Detector	A_{vw} $(\times 10^5)$	σ_{vw} $(\times 10^5)$	t_{start} (μs)
1	6.3	1.1	49.111
3	6.5	1.8	36.015
6	3.6	2.5	31.649
12	4.1	2.9	25.101
13	4.1	2.1	29.467
14	4.6	1.9	27.284
15	5.1	2.7	29.467
16	6.0	3.0	25.101
17	9.2	2.0	25.101
22	6.3	2.2	25.101
23	6.0	2.6	25.101
avg	3.3	2.3	31

disappears when the complex Fourier spectrum is averaged. The spikes near 229 kHz are slightly shifted (approximately 12 kHz) with respect to the fitted $(g-2)$ frequency and is the remnant of the interference between the CBO and the $(g-2)$ wiggle.

4.2.4 *Consistency among Detectors*

The fitted parameters and the reduced χ^2 for the individual detectors are shown in fig. 11. The reduced χ^2's are consistent with each other with a probability of 91%. The values for R are consistent on a 17% level and yield an average value $R = 143.302 \pm 1.232$. This value is consistent with the value obtained by averaging the results for the "clean" sum and detectors 1 and 4 individually: $R = 143.262 \pm 1.257$. Based on the difference in the errors (which is a lower limit in this case), these results are allowed to deviate by 0.25 ppm.

The consistency between the individual lifetimes and muon loss fractions is more problematic, but as shown earlier the normalization, muon lifetime, muon loss fraction and muon loss lifetime are very strongly correlated. The only true reason for concern is the average value of the χ^2, which is a little more than 3σ different from 1. The residuals show that there are two candidates to explain this shift, *viz.* the vertical waist and the flashlets. For a fast varying signal, the increase in the χ^2 is approximately $\Delta\chi^2 \simeq \sum \frac{A^2(t_i)}{2\,f(t_i)}$. Yannis showed with a simulation that these effects raised the reduced χ^2 by 0.011 in the case of Cenaps analysis. Under the assumption that that similation is valid for this analysis as well the deviation from 1 is lowered to just 1σ, which is acceptable.

4.3 *Systematic Errors*

The main method to estimate the systematic error related to this analysis is based on a manual χ^2 minimization.

4.3.1 *Energy Scale Corrections*

The uncertainty caused by corrections to the energy scale was obtained by fitting the data with and without an scale correction. The difference between both results was 0.04 ppm. Since the parameters describing the scale corrections are known with a 30% uncertainty, a 0.013 ppm uncertainty in R can be attributed due to this correction.

When the "clean" sum is fitted, no gain correction is applied. In that case, the entire difference of 0.04 ppm is used an the systematic error.

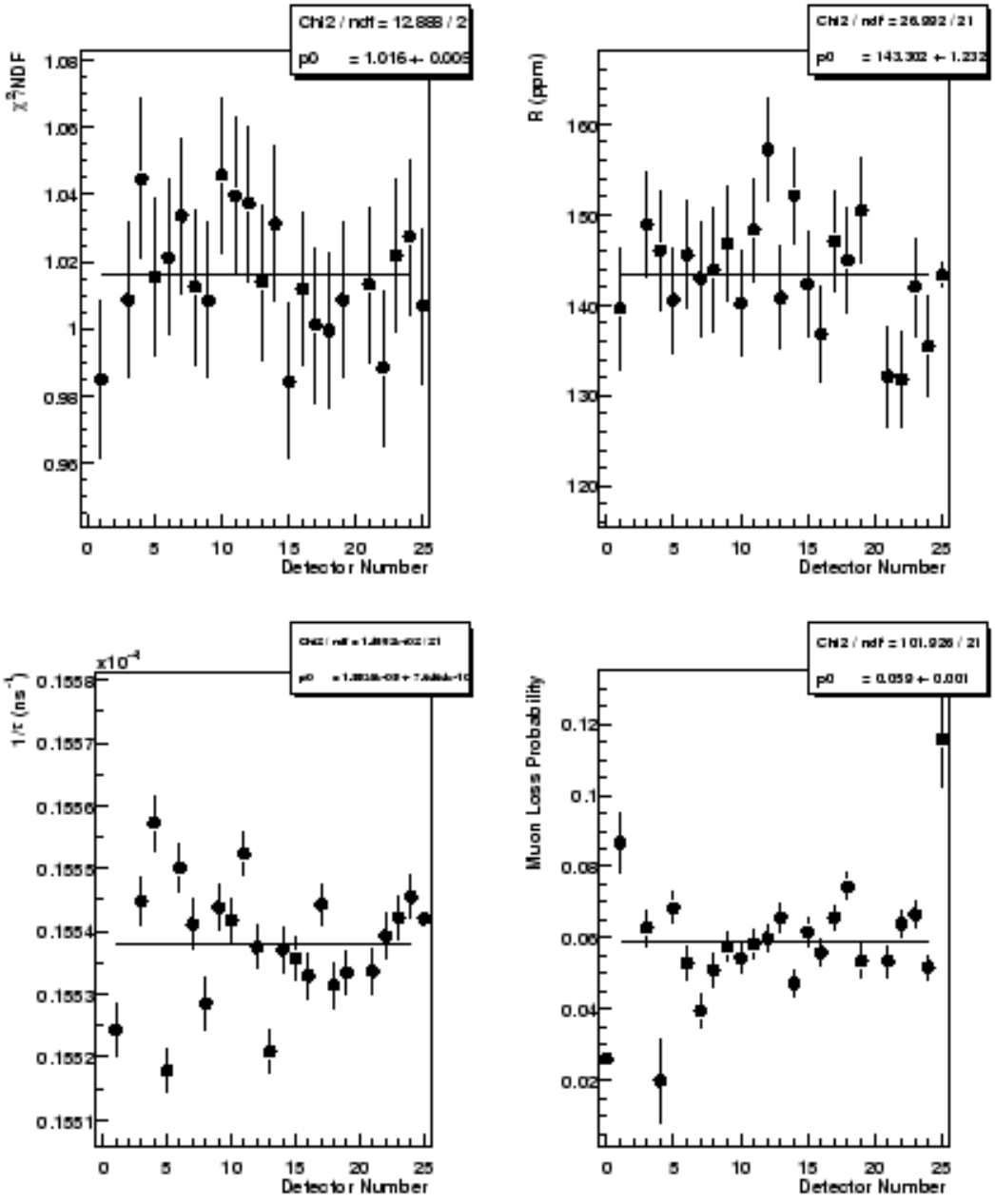

Figure 11. Selection of the fitted values which are presumably the same for all detectors. The full sum is detector 1; the "clean" sum detector 25.

4.3.2 *Coherent Betatron Oscillations*

The method used to obtain the CBO frequency and envelope parameters is described on page 18. The systematic error due to the uncertainty in the CBO frequency is less than a part per billion. The error related to the envelope parameters amounts to 0.003 ppm. The systematic shift of 0.03 ppm quoted in the analysis summary was based on a not optimal sets of parameters used in the systematic error study. This has been corrected, so that the CBO related systematic error is now reduced to 0.003 ppm.

4.3.3 *Muon Losses*

The uncertainty due to muon loss is estimated by manually scanning over the muon loss lifetime. From the dependence of the χ^2 and R, the uncertainty in this parameter can be estimated as well as the corresponding systematic error in R. For the value used ($\tau_\Lambda = 31.2 \pm 1.1$ μs), the uncertainty in R is 0.001 ppm. The discrepancy between the value obtained by David Hertzog in studying the FSD's (27.46 μs) and the value used in this analysis leads to a difference in R of 0.004 ppm. To be on the safe side, the sum of the two used as the final systematic error.

When the "clean" sum and detectors 1 and 4 are averaged, the systematic error is even smaller, because in that case the muon loss lifetime can be fitted so that the uncertainty is incorporated in the fitting error of R. The systematic error introduced by fitting detectors 1 and 4 independently is negligible.

4.3.4 *Fitting Start Time*

The error associated with the fit start times is estimated from the difference in the fitted value for R a quarter period before and after the start time used for the final result. A 0.13 and 0.35 ppm difference was observed for the 22 detector average and the average of the "clean" sum and detectors 1 and 4, respectively (statistically, 0.23 and 0.46 ppm are acceptable). The uncertainty in the locations of a zero crossing is one bin width of 150 ns, so under the assumption that phase pulling is sinusoidal and in phase with the $(g-2)$-wiggle, a systematic error of $\frac{1}{2}\omega_a \times 150 = 0.014$ ppm (0.038 ppm) can be used as the systematic error introduced by the uncertainty in the start time.

4.3.5 *Pileup Subtraction*

The uncertainty due to pileup subtraction is obtained by changing the pileup subtraction coefficients and thus include various amounts of pileup (see page 5). The resulting data is fitted as if there is no pileup (including the modification of the χ^2 calculation). This study was done for the "clean" sum and a single seed. It was found that the minimum

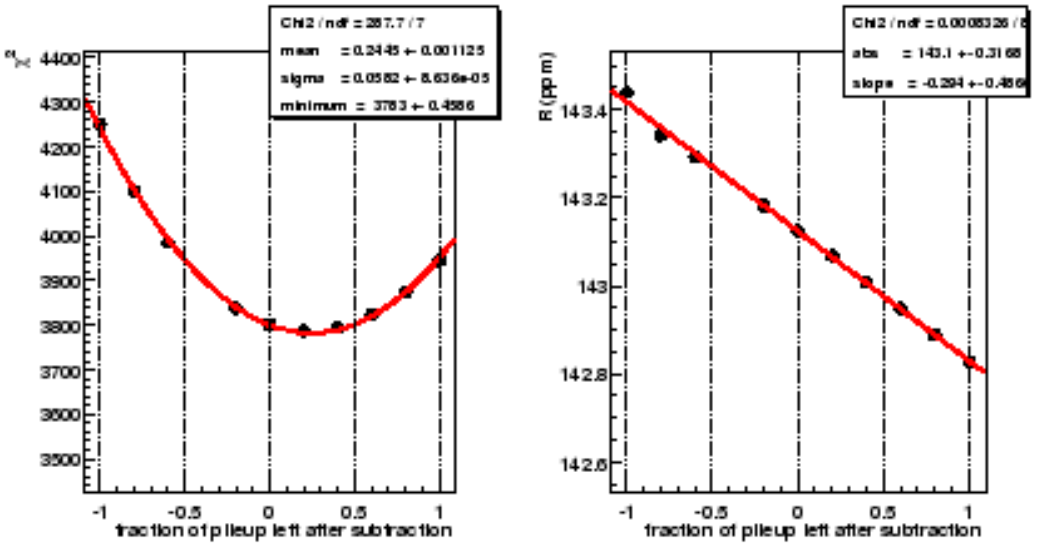

Figure 12. Minimization of χ^2 as a fuction of the fraction of pileup left after subtraction.

χ^2 was found when only about $(75 \pm 6)\%$ of the pileup was subtracted. This difference with respect to the ideal conditions leads to a shift in R of 0.071 ppm, an uncertainty of 0.017 ppm and an increase of the reduced χ^2 by 0.005.

4.3.6 *Other sources and Summary*

The systematic error introduced by the presence of fast rotation is entirely due to the limited number of random seeds used to randomize the data. For this analysis, it is found that randomization with a single sequency leads to a statistical systematic error of 8% of the statistical error of the fitting result. When 10 random number sequences are used, this error goes down by $\sqrt{10}$, to yield a total systematic error of 3.2% of the statistical error. For a result with an error of 1.3 ppm, this is a 0.04 ppm systematic error.

In table 9, the systematic error is split into its different sources. The largest systematic errors are due to pileup and randomization.

5 Conclusion

In this report, the Illinois effort to analyze the $(g-2)$ data taken in 1999 is presented. The data preparation and analysis were done using the ROOT based progam `G2Too`, that was developped at the University of Illinois in collaboration with the University of Minnesota. The full set of runs selected by Ernst Sichtermann were used. Further quality control was

Table 9
Systematic error specific to the present analysis.

Systematic Error	Value (ppm)	
	Avg	"Clean" sum
Fitting start time (phase pull peak-to-peak)	0.014	0.038
Muon Loss	0.005	–
Energy Scale	0.013	<0.04
Fast Rotation	0.031	0.032
Coherent betatron oscillation		0.003
pileup subtraction		0.071
Total (quadrature)	0.080	<0.095

done on an individual fill basis, which were checked for missing or low T0 signals in which case the whole AGS cycle was discarded and for problems with the quadrupoles or readout.

The energy and time of the decay positrons were reconstructed with the most recent version of the MilliFitter pulse finding algorithm, which uses a constant number of samples and fixed WFD sample errors. Fill randomization based on 10 sequences was applied. Pileup subtraction is based on the use of different artificial deadtimes. The presented result is obtained for an energy threshold of 2 GeV and an upper energy threshold of 6.2 GeV.

Two fitting schemes were explored. The *Illinois Method* (IM) fits individual detectors from the earliest time that reliable results are obtained and averages the results. The *Hybrid Method* (HM) fits the sum of all "good" detectors (t_{start} = 31.649 μs) and the "bad" detectors (1 and 4) individually, after which the results are averaged. An acceptable fit for the sum of all detectors required the use of a very late start time; consequently, the result, while consistent in R, does not produce a competitive uncertainty.

The fitting function accounts for $(g-2)$, coherent horizontal betatron oscillations (CBO), muon loss (ML) and time dependent variations in the energy scale (ESC). Most of the parameters used to describe these phenomena are derived from separate analyses and fixed. This includes the energy scale corrections, the CBO envelope and frequency and (mostly) the muon loss time scale. Parameters that are always fitted are the $(g-2)$ frequency (R), the normalization constant (N), the (inverse of the) muon lifetime k, the asymmetry and the $(g-2)$ phase (A_c and A_s), as well as the CBO phase and amplitude ($\hat{A}_c$ and $\hat{A}_s$) and the muon loss probability (A_Λ). The χ^2 is directly calculated as $(N-f)^2 / \left(f \times [1+Ae^{-4/\tau}]\right)$, where $[1+Ae^{-4/\tau}]$ accounts for pileup subtraction.

The results for R and χ^2 are listed below, as well as the analysis specific systematic error which is dominated by that introduced by the pileup subtraction. No systematic trending with start time is observed (mean of the modified Kawall formula is consistent with zero).

Table 10
Final results from this analysis.

	$\langle R \rangle$ (ppm)	$\langle \chi^2 \rangle$	$\sigma_{syst.}$ (ppm)	μ_{Kawall}
IM	143.302 ± 1.232	1.016 ± 0.005	0.083	$(1.5 \pm 7.6) \times 10^{-3}$
HM	143.262 ± 1.257	1.012 ± 0.013	0.099	$(1.3 \pm 3.0) \times 10^{-2}$

The χ^2's are consistent with 1 after corrections for known omissions and imperfections in the fitting function are made. The preferred result is that from the IM.

A: Gains and Timing

Table 11
Gains and time offsets for all detectors.

Detector	Gain (GeV/ADC)	Time Offset (ns)
1	472.66	18.761503
2	454.05	9.728187
3	475.91	-5.558964
4	466.95	-12.507669
5	473.55	-20.151244
6	483.31	-12.507669
7	506.91	-8.338446
8	487.15	22.235855
9	519.05	11.812798
10	470.37	31.269172
11	456.05	36.133265
12	443.05	61.843473
13	469.71	60.453732
14	469.85	77.130623
15	482.01	81.299846
16	481.25	92.417774
17	475.53	91.722904
18	452.97	70.876789
19	464.14	63.928084
20	360.56	44.471711
21	459.47	43.081970
22	454.38	22.930726
23	457.04	20.151244
24	464.80	4.86409

Table 12
Parameters used to describe the variation of the average energy ($2 < E < 6$ GeV) with time. The time at which the fit was started is given as well. From this time on, the functional form given in eq. 15 gave an adequate description of the data.

Det.	$N_1 \times 10^3$	τ_1 (μs)	$N_2 \times 10^3$	τ_2 (μs)	t_{start} (μs)
1	-9.90	30.03	–	–	50
3	0.56	18.33	–	–	28
4	-0.12	18.73	–	–	34
5	-2.90	22.24	–	–	37
6	1.51	30.53	–	–	33
7	-9.96	15.43	5.69	19.54	20
8	18.94	30.30	-14.38	35.24	20
9	20.84	23.97	-15.32	27.35	20
10	-1.95	5.57	–	–	20
11	16.62	5.55	–	–	20
12	1.26	27.22	–	–	20
13	-560.21	2.84	–	–	20
14	47.95	42.33	-45.48	44.60	20
15	0.34	15.50	–	–	20
16	-0.13	15.47	–	–	20
17	130.36	83.30	-130.05	83.79	20
18	-2.09	541.54	–	–	20
19	-0.74	101.75	–	–	20
21	-0.99	305.07	–	–	20
22	14.00	16.77	-8.91	20.58	20
23	38.31	4.74	–	–	20
24	21.49	17.85	-13.53	21.65	20
sum	-0.57	79.78	0.00	0.00	50

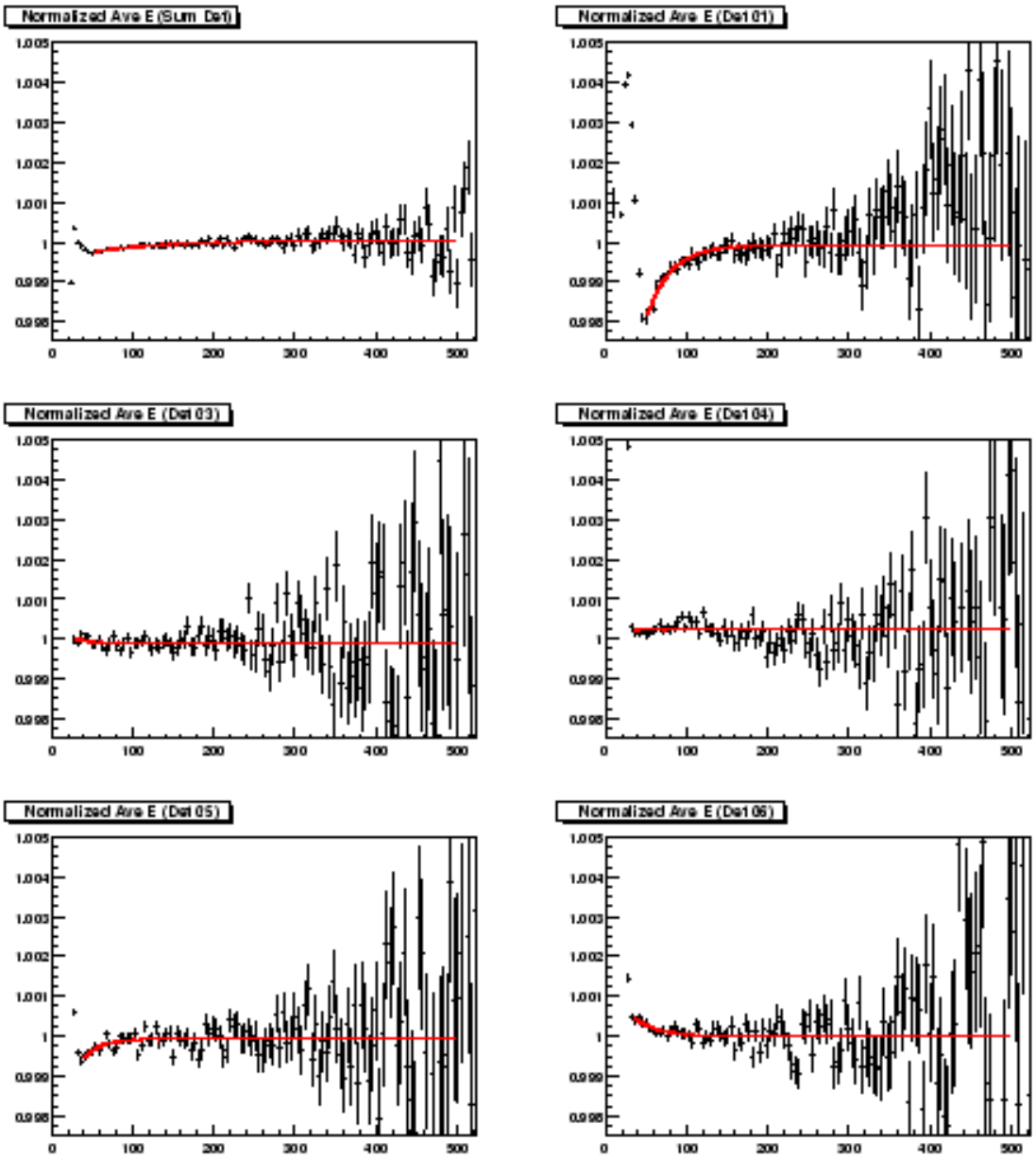

Figure 13. Change in the average energy as a function of time (detectors 1 – 6).

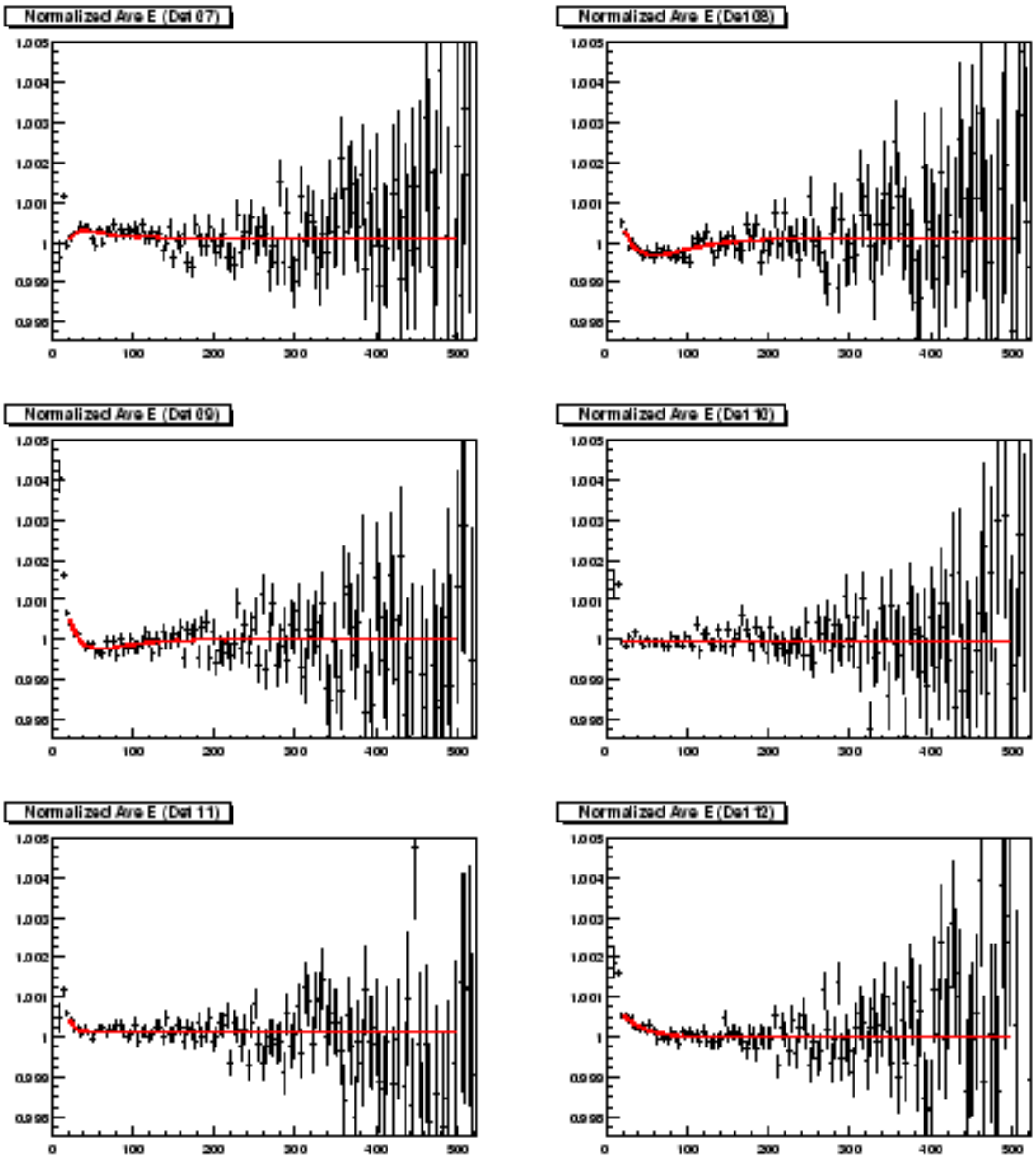

Figure 14. Change in the average energy as a function of time (detectors 7 – 12).

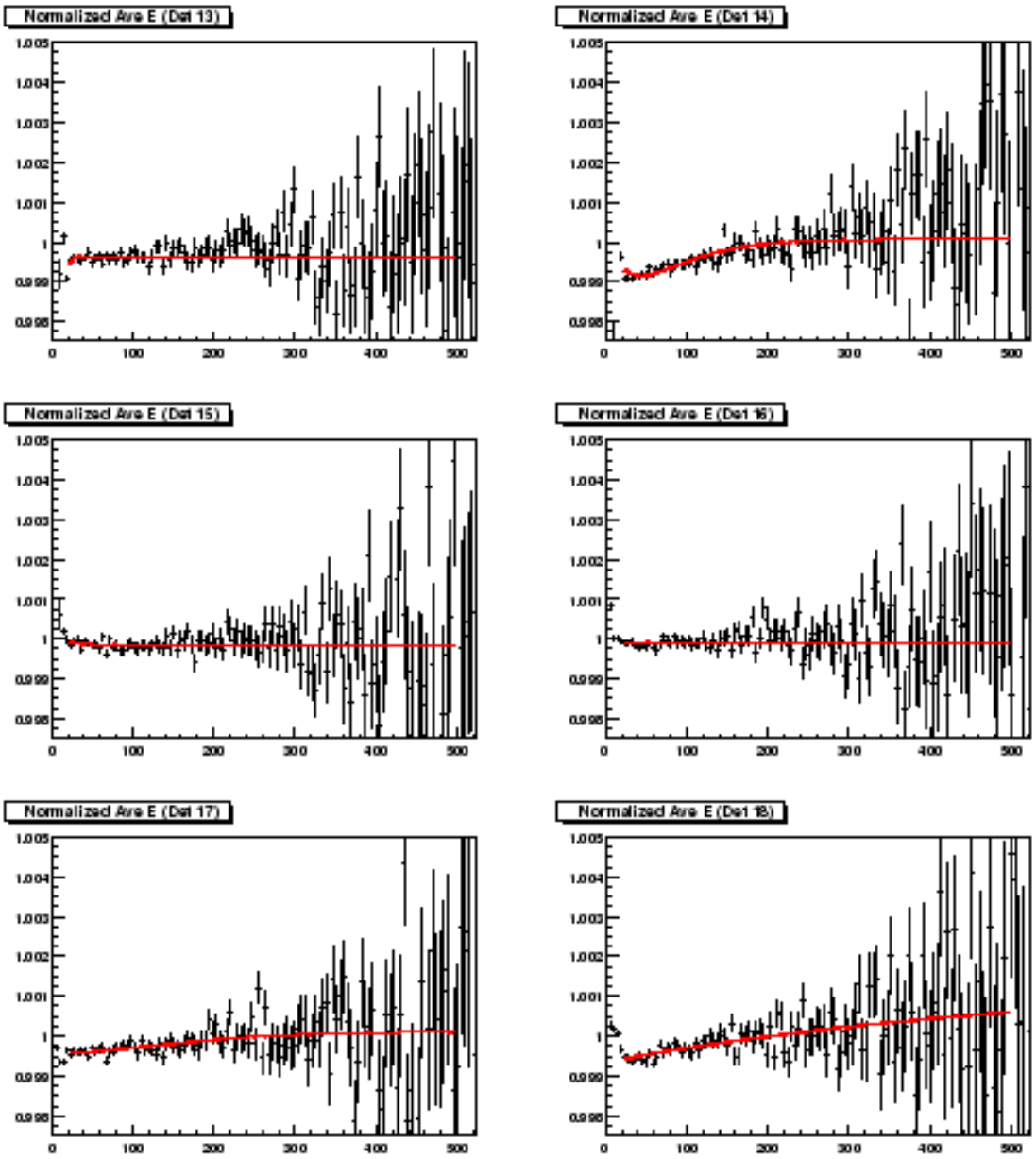

Figure 15. Change in the average energy as a function of time (detectors 13 – 18).

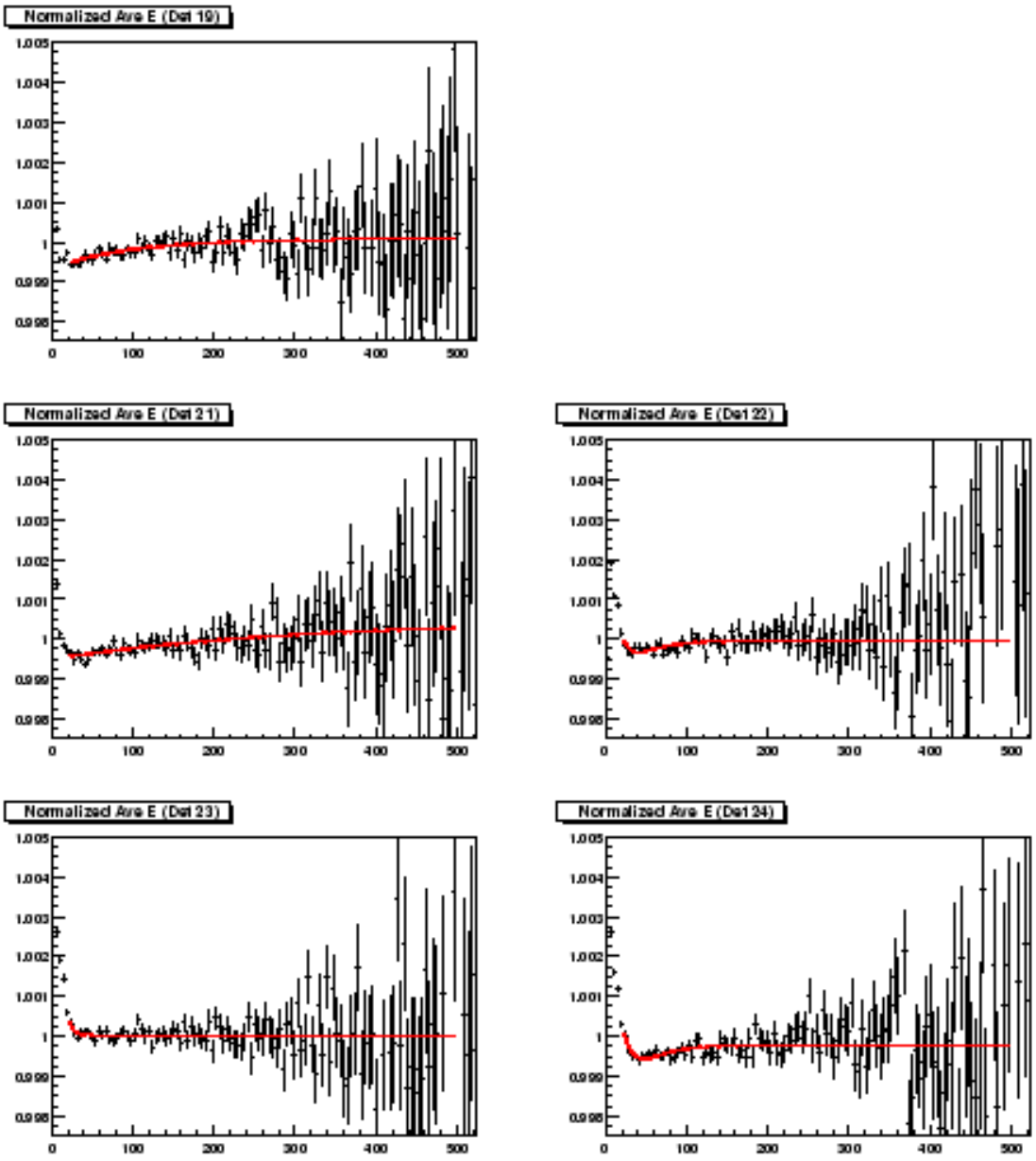

Figure 16. Change in the average energy as a function of time (detectors 19 – 24).

Table 13
Sensitivity to energy scale changes for different energy ranges. $\frac{dQ}{d(E)}$ is in Gev^{-1}, $\frac{d\phi}{dQ}$ is in mrad.

Ecut		$1.8 < E < 3.1$			$1.8 < E < 6.2$			$2.0 < E < 3.1$			$2.0 < E < 6.2$		
Det.	$\frac{dQ}{d(E)}$	$\frac{dN}{NdQ}$	$\frac{dA}{AdQ}$	$\frac{d\phi}{dQ}$	$\frac{dN}{NdQ}$	$\frac{dA}{AdQ}$	$\frac{d\phi}{dQ}$	$\frac{dN}{NdQ}$	$\frac{dA}{AdQ}$	$\frac{d\phi}{dQ}$	$\frac{dN}{NdQ}$	$\frac{dA}{AdQ}$	$\frac{d\phi}{dQ}$
1	2.13	1.99	0.66	68.1	2.18	1.08	55	2.69	1.29	65.2	2.95	1.81	52.4
2	2.17	2.02	0.54	-97.7	2.24	1.04	-79.6	2.67	1.16	-88.9	2.97	1.77	-72.1
3	2.19	2.09	0.74	-99.3	2.27	1.14	-85.5	2.82	1.38	-105	3.06	1.87	-92.6
4	2.15	2.11	0.84	-79.6	2.26	1.15	-78.5	2.81	1.51	-64.4	3.02	1.89	-66
5	2.16	2.09	0.74	-107.3	2.26	1.12	-95.6	2.79	1.40	-97.5	3.03	1.85	-87.3
6	2.22	2.18	0.84	-118.2	2.35	1.22	-100.9	2.89	1.49	-107.1	3.13	1.96	-90.6
7	2.52	2.84	1.65	36.7	2.92	1.82	36	3.68	2.49	25.1	3.80	2.71	25.1
8	2.65	3.04	1.80	-50.4	3.11	1.94	-48	3.94	2.74	-30	4.04	2.92	-27.8
9	2.57	3.13	2.00	16	3.13	2.05	15.9	4.15	3.05	14.8	4.14	3.12	14.4
10	2.17	2.17	0.88	42.5	2.31	1.20	37.7	2.87	1.54	24.4	3.07	1.94	20.3
11	2.16	2.09	0.81	28.1	2.26	1.19	21.6	2.78	1.45	26.8	3.02	1.91	19.8
12	2.23	2.17	0.84	46	2.35	1.24	37.4	2.87	1.50	44.4	3.12	2.00	35.5
13	2.13	2.01	0.66	66.1	2.19	1.07	55.3	2.73	1.30	58.2	2.97	1.80	48
14	2.17	2.17	0.90	-12	2.31	1.23	-10.3	2.88	1.55	-15.3	3.09	1.95	-13.6
15	2.12	2.02	0.69	78.5	2.19	1.07	66.7	2.76	1.36	66.9	2.99	1.81	56
16	2.25	2.28	0.91	-7.7	2.42	1.23	-9.1	3.01	1.62	3.7	3.21	2.01	1.6
17	2.13	2.07	0.69	-15.6	2.23	1.06	-18.5	2.77	1.33	-7.1	2.99	1.79	-11.9
18	2.21	2.12	0.65	-0.9	2.31	1.09	-3.9	2.83	1.31	-2.1	3.09	1.84	-6
19	2.17	2.02	0.55	-53.8	2.22	1.02	-46.6	2.73	1.18	-50.4	3.00	1.74	-44.7
20	2.78	1.44	-0.42	-142.2	1.70	0.64	-65.8	1.51	-0.41	-89.3	1.89	0.83	-46.2
21	2.18	2.12	0.72	-75.8	2.29	1.10	-77.3	2.84	1.37	-60.6	3.08	1.84	-66.8
22	2.25	2.20	0.84	-69.2	2.38	1.22	-59.3	2.90	1.50	-77.8	3.15	1.97	-68.3
23	2.23	2.22	1.20	101.1	2.42	1.54	100.4	2.91	1.72	73.8	3.20	2.16	88.2
24	2.25	2.13	0.69	-54.2	2.34	1.16	-43.3	2.81	1.34	-52.8	3.10	1.91	-42.4
sum	2.22	2.20	0.89	-8.15	2.36	1.25	-8.71	2.92	1.55	-9.16	3.15	1.99	-9.59

B: Pileup Related Parameters

Table 14
Parameters used to describe the enhancement of pileup due to fast rotation.

Det	A_ϵ	$t\epsilon$ (μs)	σ_ϵ (μs)	$A_\epsilon^{(2)} \times 10^3$	$t_\epsilon^{(2)}$ (μs)	$\sigma_\epsilon^{(2)}$ (μs)
1	1.194	-4.271	13.67	3.037	53.23	7.355
3	1.387	-4.304	13.32	2.792	52.73	9.498
4	1.249	-4.377	13.60	2.828	53.00	8.119
5	1.408	-4.284	13.28	2.809	53.20	8.973
6	1.375	-4.311	13.33	2.728	52.85	9.728
7	1.193	-4.274	13.67	2.980	53.88	7.041
8	1.207	-4.258	13.63	2.932	54.00	6.792
9	1.182	-4.294	13.70	3.007	53.40	6.999
10	1.172	-4.309	13.72	2.846	53.52	6.969
11	1.207	-4.273	13.64	2.771	53.24	8.429
12	1.198	-4.249	13.67	2.964	53.81	7.127
13	1.208	-4.260	13.63	2.887	53.25	7.318
14	1.200	-4.261	13.66	3.032	53.36	6.954
15	1.195	-4.284	13.67	2.977	53.64	7.520
16	1.169	-4.282	13.75	3.121	53.30	6.754
17	1.169	-4.287	13.75	3.210	53.78	6.622
18	1.200	-4.203	13.69	3.216	53.05	6.785
19	1.190	-4.268	13.68	2.867	53.28	7.023
21	1.177	-4.272	13.71	2.933	53.75	6.808
22	1.202	-4.268	13.65	2.882	53.75	7.482
23	1.225	-4.233	13.59	3.174	53.52	7.223
24	1.202	-4.277	13.64	2.926	53.62	7.573
avg	1.223	-4.277	13.62	2.951	53.42	7.462

Table 15
Results for the phase shift between the normal and pileup component. This study was done using the old version of MilliFitter.

Ecut	$1.8 < E < 3.1$ GeV	$1.8 < E < 6.2$ GeV	$2.0 < E < 3.1$ GeV	$2.0 < E < 6.2$ GeV
Det.		$\Delta\phi_1$ (mrad)		
1	0.0 ± 20.4	25.0 ± 35.3	14.8 ± 1.4	–
2	15.6 ± 10.4	31.2 ± 31.8	18.8 ± 11.1	75.0 ± 114.6
3	3.1 ± 10.7	75.0 ± 55.8	3.1 ± 17.2	–
4	-3.1 ± 13.3	25.0 ± 51.2	3.1 ± 15.8	-175.0 ± 447.7
5	-10.9 ± 12.3	6.2 ± 42.0	-20.3 ± 9.2	43.8 ± 18.2
6	12.5 ± 12.2	106.2 ± 58.6	12.5 ± 15.6	-100.0 ± 181.6
7	-21.9 ± 17.7	25.0 ± 66.6	-12.5 ± 47.6	-9.4 ± 24.2
8	-3.1 ± 22.0	12.5 ± 51.9	25.0 ± 99.2	-12.5 ± 17.0
9	31.2 ± 18.6	-100.0 ± 89.8	37.5 ± 20.7	-18.8 ± 28.0
10	25.0 ± 13.7	75.0 ± 106.4	25.0 ± 15.1	–
11	-6.2 ± 12.7	25.0 ± 37.9	-9.4 ± 16.8	-150.0 ± 596.3
12	-28.1 ± 11.6	-50.0 ± 56.1	-21.9 ± 15.9	-75.0 ± 188.3
13	-14.1 ± 10.6	-31.2 ± 10.3	-6.2 ± 12.0	–
14	6.2 ± 17.2	37.5 ± 46.2	18.8 ± 13.0	-150.0 ± 81.0
15	-1.6 ± 9.0	-12.5 ± 37.3	-3.1 ± 17.1	–
16	-4.7 ± 5.5	-62.5 ± 66.3	-12.5 ± 14.5	75.0 ± 149.3
17	6.2 ± 8.0	37.5 ± 53.5	12.5 ± 4.1	–
18	3.1 ± 18.1	50.0 ± 86.5	12.5 ± 12.7	-175.0 ± 108.9
19	-6.2 ± 11.6	-6.2 ± 42.3	0.0 ± 14.4	–
20	12.5 ± 45.8	50.0 ± 186.0	-37.5 ± 50.1	-50.0 ± 119.4
21	15.6 ± 16.1	100.0 ± 17.9	15.6 ± 18.0	-175.0 ± 93.3
22	3.1 ± 2.6	50.0 ± 86.7	6.2 ± 11.5	-100.0 ± 58.0
23	9.4 ± 21.8	125.0 ± 93.4	12.5 ± 61.1	–
24	1.6 ± 6.1	12.5 ± 57.1	6.2 ± 19.7	-75.0 ± 189.6
avg	1.4 ± 1.7	8.4 ± 6.9	12.9 ± 1.2	15 ± 83
sum	0.8 ± 1.6	34.4 ± 13.3	4.7 ± 5.6	-75.0 ± 30.2

C: Muon Loss

Table 16

Time dependent muon loss term per lifetime for start times as early as possible ($\tau_\Lambda = 27.46\ \mu$s). The old version of MilliFitter was used for this study.

Ecut	$1.8 < E < 3.1$ GeV	$1.8 < E < 6.2$ GeV	$2.0 < E < 3.1$ GeV	$2.0 < E < 6.2$ GeV
Det.	A_Λ (%/per muon lifetime)			
1	9.4 ± 1.9	9.1 ± 1.8	11.7 ± 2.2	11.5 ± 2.1
2	–	–	–	–
3	1.8 ± 0.9	2.8 ± 0.9	1.2 ± 1.0	2.6 ± 1.0
4	3.5 ± 1.2	4.7 ± 1.3	3.0 ± 1.5	4.7 ± 1.5
5	6.1 ± 2.0	7.5 ± 1.9	4.2 ± 2.2	6.1 ± 2.3
6	11.2 ± 2.0	12.4 ± 1.9	11.7 ± 2.3	13.1 ± 2.3
7	7.0 ± 2.3	7.0 ± 2.3	11.2 ± 2.7	11.2 ± 2.6
8	–	–	0.5 ± 0.9	0.5 ± 0.9
9	–	–	–	0.1 ± 1.6
10	2.6 ± 1.3	3.0 ± 1.2	2.8 ± 1.5	3.3 ± 1.5
11	3.9 ± 0.6	4.3 ± 0.6	3.8 ± 0.6	4.2 ± 0.6
12	1.4 ± 0.6	2.1 ± 0.6	2.3 ± 0.7	3.0 ± 0.7
13	6.6 ± 0.6	6.8 ± 0.5	6.1 ± 0.6	6.6 ± 0.6
14	6.7 ± 0.6	7.1 ± 0.6	6.7 ± 0.7	7.3 ± 0.7
15	8.7 ± 0.6	8.8 ± 0.5	8.7 ± 0.6	8.8 ± 0.6
16	6.3 ± 0.6	6.6 ± 0.6	6.0 ± 0.7	6.3 ± 0.7
17	6.3 ± 0.6	6.6 ± 0.6	5.3 ± 0.6	5.6 ± 0.6
18	10.3 ± 0.6	10.4 ± 0.6	10.3 ± 0.7	10.3 ± 0.7
19	6.3 ± 0.6	6.7 ± 0.6	6.2 ± 0.6	6.6 ± 0.7
20	–	–	–	14.9 ± 0.7
21	6.8 ± 0.6	6.9 ± 0.6	6.3 ± 0.6	6.6 ± 0.7
22	6.1 ± 0.6	6.3 ± 0.6	6.0 ± 0.7	6.1 ± 0.7
23	4.7 ± 0.6	4.9 ± 0.6	4.3 ± 0.7	4.7 ± 0.6
24	2.8 ± 0.6	3.2 ± 0.6	1.9 ± 0.7	2.3 ± 0.7
avg	5.75 ± 0.15	6.09 ± 0.15	5.34 ± 0.17	6.21 ± 0.16
sum	4.2 ± 0.5	4.8 ± 0.5	3.9 ± 0.6	4.6 ± 0.6

Table 17
Time dependent muon loss term per lifetime for start times 24.2 μs later than as early as possible. The old version of MilliFitter was used for this study.

Ecut	$1.8 < E < 3.1$ GeV	$1.8 < E < 6.2$ GeV	$2.0 < E < 3.1$ GeV	$2.0 < E < 6.2$ GeV
Det.	A_A (%/muon lifetime)			
1	–	–	–	–
2	–	–	–	–
3	–	–	1.4 ± 3.2	1.9 ± 3.1
4	–	–	–	–
5	9.4 ± 6.0	12.2 ± 5.9	5.6 ± 6.8	9.4 ± 6.7
6	–	–	–	–
7	11.2 ± 6.8	13.1 ± 7.1	–	–
8	–	–	–	–
9	–	–	–	–
10	13.1 ± 3.9	14.1 ± 3.8	11.2 ± 4.5	12.2 ± 4.5
11	5.2 ± 1.8	5.6 ± 1.8	3.8 ± 2.1	4.7 ± 2.1
12	7.0 ± 1.8	8.0 ± 1.8	5.6 ± 2.2	6.8 ± 2.1
13	3.5 ± 1.7	3.8 ± 1.8	1.9 ± 2.1	2.3 ± 2.0
14	3.3 ± 1.8	3.8 ± 1.8	2.3 ± 2.1	2.8 ± 2.1
15	9.6 ± 1.8	9.6 ± 1.8	10.8 ± 2.1	10.8 ± 2.0
16	7.5 ± 1.8	7.5 ± 1.8	7.5 ± 2.1	7.5 ± 2.2
17	7.0 ± 1.8	7.7 ± 1.7	7.0 ± 2.1	7.7 ± 2.1
18	12.7 ± 2.0	12.7 ± 2.0	13.1 ± 2.3	13.1 ± 2.3
19	5.4 ± 1.8	5.9 ± 1.7	4.5 ± 2.0	5.2 ± 2.1
20	–	–	–	–
21	7.5 ± 1.8	7.7 ± 1.8	7.5 ± 2.1	8.0 ± 2.1
22	7.0 ± 1.9	7.0 ± 1.9	8.0 ± 2.2	8.4 ± 2.2
23	3.5 ± 1.7	4.0 ± 1.8	2.3 ± 2.1	–
24	2.1 ± 1.8	2.8 ± 1.8	0.9 ± 2.2	1.6 ± 2.1
avg	6.30 ± 0.49	6.71 ± 0.49	5.64 ± 0.57	6.46 ± 0.59
sum	2.8 ± 1.6	3.8 ± 1.5	1.9 ± 1.8	3.0 ± 1.8

D: Coherent betatron motion

Table 18

CBO Frequency for start times as early as possible; $\sigma_\beta = 100\,\mu$s, $t_\beta = 0$. The old version of MilleFitter was used for this study.

Ecut	$1.8 < E < 3.1$ GeV	$1.8 < E < 6.2$ GeV	$2.0 < E < 3.1$ GeV	$2.0 < E < 6.2$ GeV
Det.		$\omega_\beta/2\pi$ (kHz)		
1	470.12 ± 0.12	470.04 ± 0.11	470.39 ± 0.12	470.37 ± 0.12
2	470.51 ± 0.09	470.60 ± 0.09	470.56 ± 0.11	470.71 ± 0.11
3	470.77 ± 0.07	470.73 ± 0.07	470.60 ± 0.09	470.55 ± 0.09
4	470.31 ± 0.11	470.34 ± 0.11	470.27 ± 0.12	470.30 ± 0.12
5	470.34 ± 0.17	470.34 ± 0.16	470.23 ± 0.15	470.23 ± 0.13
6	470.80 ± 0.14	470.83 ± 0.13	470.66 ± 0.12	470.70 ± 0.12
7	470.41 ± 0.07	470.38 ± 0.07	470.30 ± 0.07	470.26 ± 0.07
8	470.36 ± 0.04	470.37 ± 0.04	470.44 ± 0.04	470.45 ± 0.04
9	470.52 ± 0.04	470.52 ± 0.04	470.60 ± 0.05	470.61 ± 0.05
10	470.78 ± 0.09	470.80 ± 0.09	470.62 ± 0.08	470.62 ± 0.07
11	470.52 ± 0.08	470.43 ± 0.07	470.33 ± 0.07	470.27 ± 0.07
12	470.03 ± 0.08	470.10 ± 0.07	470.08 ± 0.07	470.14 ± 0.07
13	470.42 ± 0.07	470.41 ± 0.07	470.47 ± 0.08	470.46 ± 0.08
14	470.23 ± 0.06	470.23 ± 0.06	470.27 ± 0.07	470.28 ± 0.08
15	470.20 ± 0.07	470.20 ± 0.07	470.12 ± 0.07	470.12 ± 0.07
16	470.55 ± 0.08	470.55 ± 0.08	470.34 ± 0.10	470.37 ± 0.08
17	470.45 ± 0.08	470.43 ± 0.07	470.27 ± 0.08	470.26 ± 0.07
18	–	–	470.05 ± 0.08	470.09 ± 0.07
19	–	–	470.30 ± 0.07	470.31 ± 0.07
20	470.59 ± 0.03	470.55 ± 0.03	470.62 ± 0.03	470.57 ± 0.04
21	–	–	470.85 ± 0.09	470.89 ± 0.09
22	470.55 ± 0.09	470.57 ± 0.09	470.78 ± 0.10	470.81 ± 0.10
23	470.34 ± 0.07	470.34 ± 0.07	470.35 ± 0.07	470.37 ± 0.07
24	470.02 ± 0.08	470.01 ± 0.07	470.10 ± 0.07	470.08 ± 0.06
avg	470.45 ± 0.013	470.43 ± 0.014	470.43 ± 0.014	470.41 ± 0.014
sum	470.53 ± 0.08	470.58 ± 0.08	470.61 ± 0.11	470.66 ± 0.09

Table 19
CBO Lifetime for start times as early as possible; $\omega\beta/2\pi = 470.5$ kHz, $t_\beta = 0$. The old version of MilliFitter was used for this study.

Ecut	$1.8 < E < 3.1$ GeV	$1.8 < E < 6.2$ GeV	$2.0 < E < 3.1$ GeV	$2.0 < E < 6.2$ GeV
Det.		τ_β (μs)		
1	90.2 ± 3.7	94.1 ± 3.8	111.2 ± 6.9	114.4 ± 6.4
2	84.3 ± 1.9	85.9 ± 2.0	90.9 ± 3.1	92.5 ± 3.8
3	–	–	–	–
4	101.9 ± 4.5	104.2 ± 4.9	91.7 ± 4.0	94.1 ± 4.0
5	103.4 ± 6.7	103.4 ± 6.5	94.1 ± 4.9	95.6 ± 4.8
6	108.1 ± 5.1	110.5 ± 4.8	96.4 ± 3.2	98.8 ± 3.6
7	99.5 ± 2.3	99.5 ± 2.3	92.9 ± 2.0	93.3 ± 1.9
8	90.4 ± 1.3	90.0 ± 1.3	90.0 ± 1.3	89.6 ± 1.2
9	98.8 ± 1.8	98.8 ± 1.8	100.3 ± 1.8	100.3 ± 1.8
10	104.2 ± 4.3	103.4 ± 3.9	96.4 ± 3.0	96.4 ± 2.8
11	–	–	81.6 ± 2.1	82.0 ± 2.1
12	–	–	80.8 ± 1.9	80.2 ± 1.8
13	81.6 ± 1.9	81.6 ± 1.9	87.4 ± 2.4	87.0 ± 2.2
14	–	–	89.4 ± 2.5	90.5 ± 2.8
15	–	–	80.8 ± 2.1	80.4 ± 1.9
16	83.9 ± 2.3	83.1 ± 2.1	92.5 ± 2.8	91.7 ± 3.2
17	82.0 ± 2.4	81.6 ± 2.3	83.9 ± 2.6	84.3 ± 2.5
18	89.8 ± 2.7	90.5 ± 2.7	92.1 ± 2.8	92.9 ± 2.7
19	–	–	–	–
20	85.3 ± 0.9	82.5 ± 1.0	87.4 ± 1.1	83.5 ± 1.3
21	88.6 ± 2.6	87.8 ± 2.4	93.3 ± 3.3	90.9 ± 3.6
22	85.5 ± 2.6	85.5 ± 2.6	86.6 ± 3.0	86.2 ± 2.5
23	–	–	82.7 ± 2.1	83.9 ± 2.1
24	86.2 ± 3.0	87.0 ± 2.5	90.9 ± 2.7	91.3 ± 2.5
avg.	88.7 ± 0.5	88.4 ± 0.5	89.1 ± 0.5	88.5 ± 0.5
sum	95.2 ± 2.2	95.2 ± 2.3	93.3 ± 2.3	92.9 ± 2.3

Table 20
CBO Lifetime for start times 24.2 μs later than as early as possible; $\omega_\beta/2\pi = 470.5$ kHz, $t_\beta = 0$. The old version of Millifitter was used for this study.

Ecut	$1.8 < E < 3.1$ GeV	$1.8 < E < 6.2$ GeV	$2.0 < E < 3.1$ GeV	$2.0 < E < 6.2$ GeV
Det.		τ_β (μs)		
1	108.1 ± 9.3	108.1 ± 9.4	130.0 ± 5.2	126.9 ± 11.0
2	90.2 ± 2.9	88.2 ± 2.7	94.8 ± 4.1	91.7 ± 3.7
3	97.2 ± 4.2	97.2 ± 4.5	112.8 ± 8.9	114.4 ± 9.1
4	101.9 ± 6.4	101.9 ± 6.9	89.4 ± 6.0	90.9 ± 5.4
5	108.1 ± 8.8	112.8 ± 9.2	101.9 ± 7.3	109.7 ± 8.1
6	102.7 ± 5.1	101.9 ± 4.5	90.2 ± 3.3	90.2 ± 3.2
7	103.4 ± 3.1	101.1 ± 2.9	98.0 ± 2.9	95.6 ± 2.5
8	99.9 ± 1.9	99.1 ± 1.8	94.5 ± 1.6	93.9 ± 1.6
9	110.1 ± 2.6	110.1 ± 2.5	114.0 ± 2.7	114.0 ± 2.7
10	148.8 ± 11.9	144.1 ± 10.0	125.3 ± 6.9	122.2 ± 6.1
11	96.0 ± 3.7	96.4 ± 3.7	108.1 ± 5.3	109.7 ± 4.8
12	89.4 ± 3.0	90.5 ± 3.2	92.5 ± 2.4	92.5 ± 3.7
13	87.8 ± 2.5	87.8 ± 2.4	90.2 ± 2.7	90.2 ± 2.5
14	87.8 ± 2.4	88.6 ± 2.4	106.6 ± 4.5	108.1 ± 5.3
15	94.1 ± 3.5	92.5 ± 2.6	92.5 ± 2.6	90.9 ± 3.1
16	83.9 ± 3.0	85.5 ± 3.1	98.0 ± 5.5	100.3 ± 4.7
17	103.4 ± 5.1	106.6 ± 5.2	117.5 ± 8.1	119.1 ± 6.9
18	83.9 ± 2.7	86.2 ± 2.4	84.7 ± 3.1	87.8 ± 3.2
19	87.8 ± 3.7	89.4 ± 3.2	80.8 ± 2.7	82.3 ± 2.6
20	98.2 ± 1.6	96.2 ± 1.8	104.6 ± 2.1	101.5 ± 2.4
21	97.2 ± 3.8	94.8 ± 3.5	90.2 ± 3.7	87.0 ± 3.4
22	83.9 ± 3.0	85.5 ± 3.2	81.6 ± 3.1	83.1 ± 2.8
23	101.9 ± 4.0	101.1 ± 3.9	106.6 ± 4.7	105.8 ± 4.1
24	100.3 ± 4.8	98.8 ± 3.9	–	105.0 ± 2.8
avg	95.0 ± 0.6	94.7 ± 0.6	94.6 ± 0.6	94.4 ± 0.6
sum	93.7 ± 2.6	93.7 ± 2.6	81.6 ± 2.0	81.2 ± 2.1

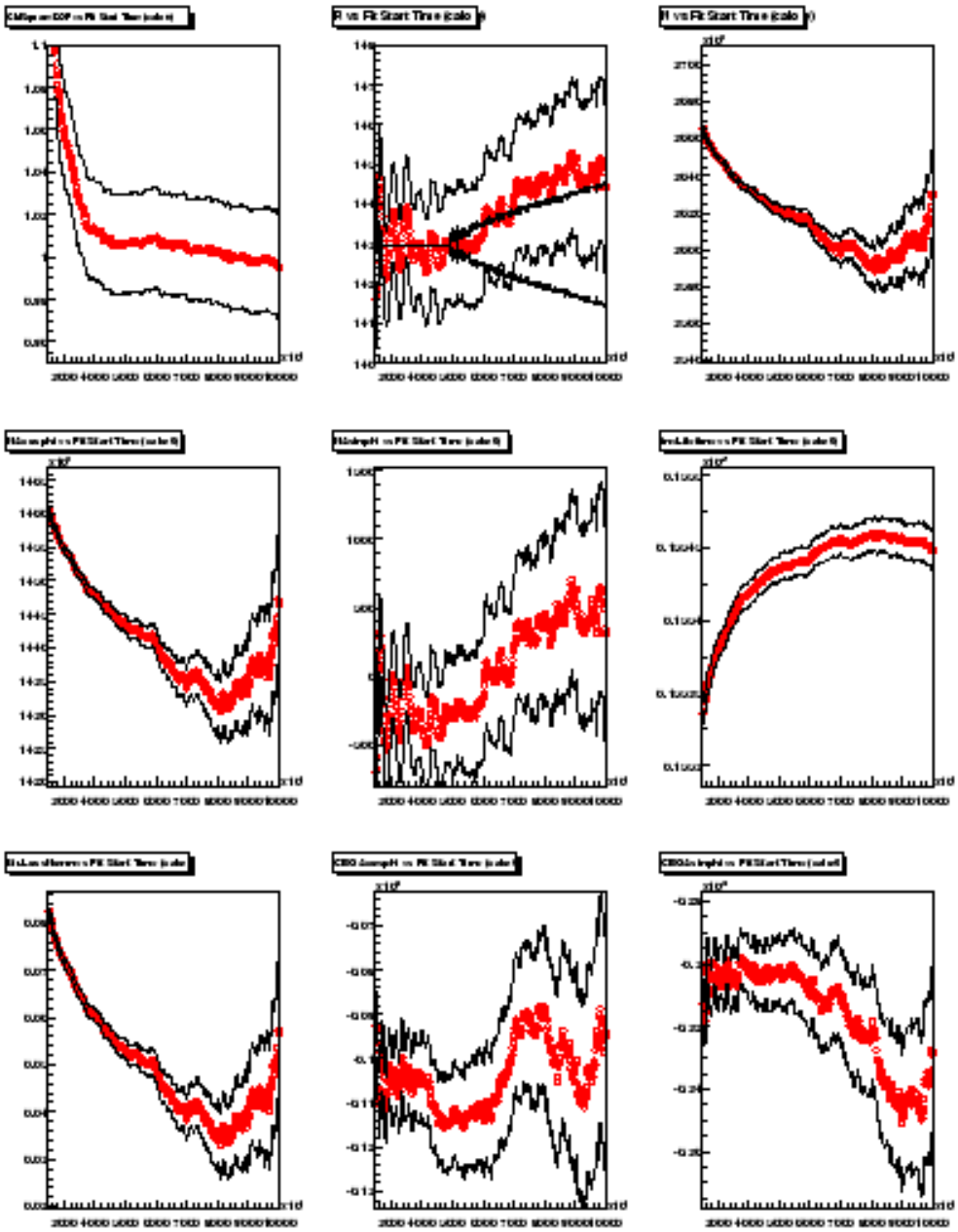

Figure 17. Results for the floated parameters for the sum of the detectors.

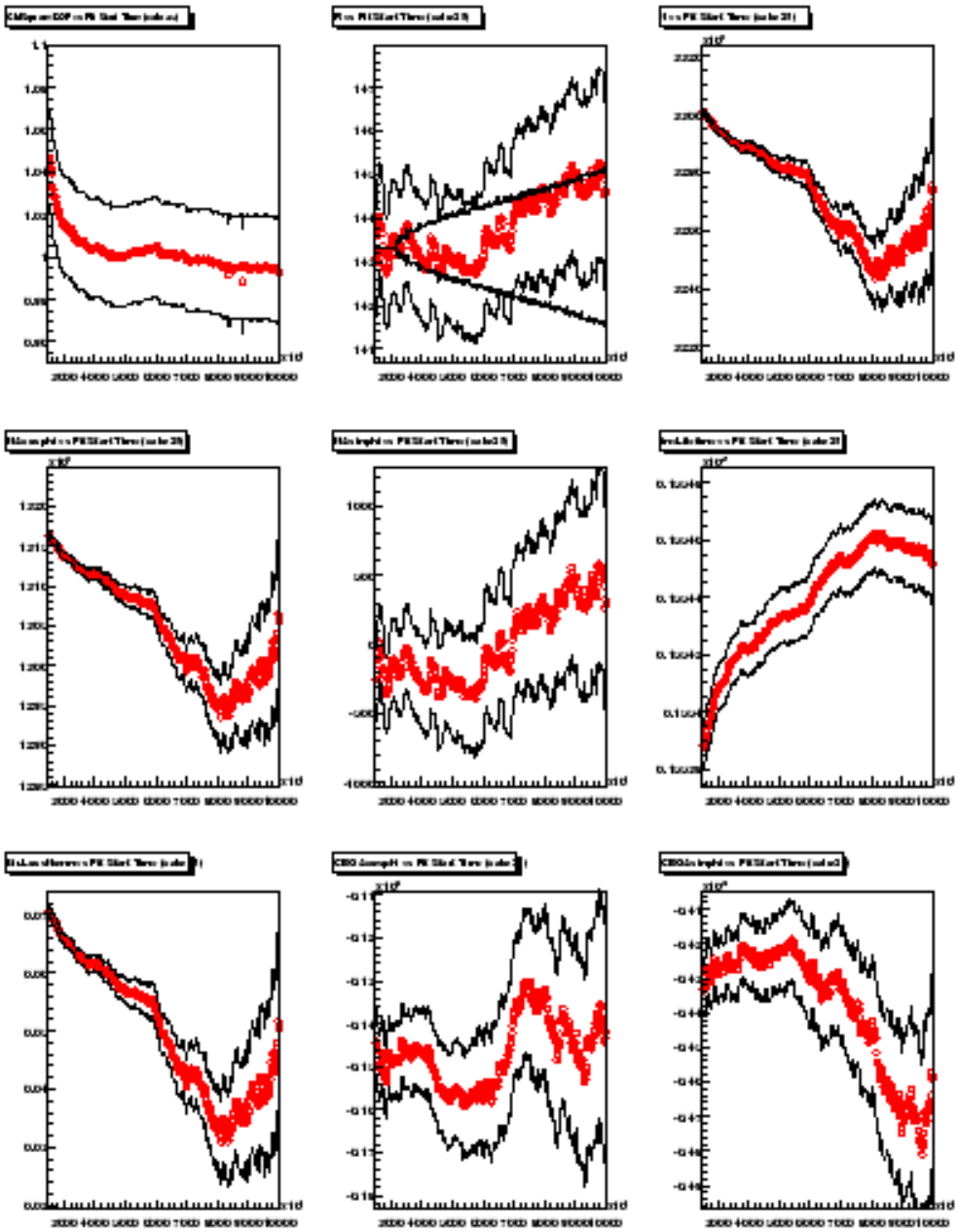

Figure 18. Results for the floated parameters for the "clean" sum.

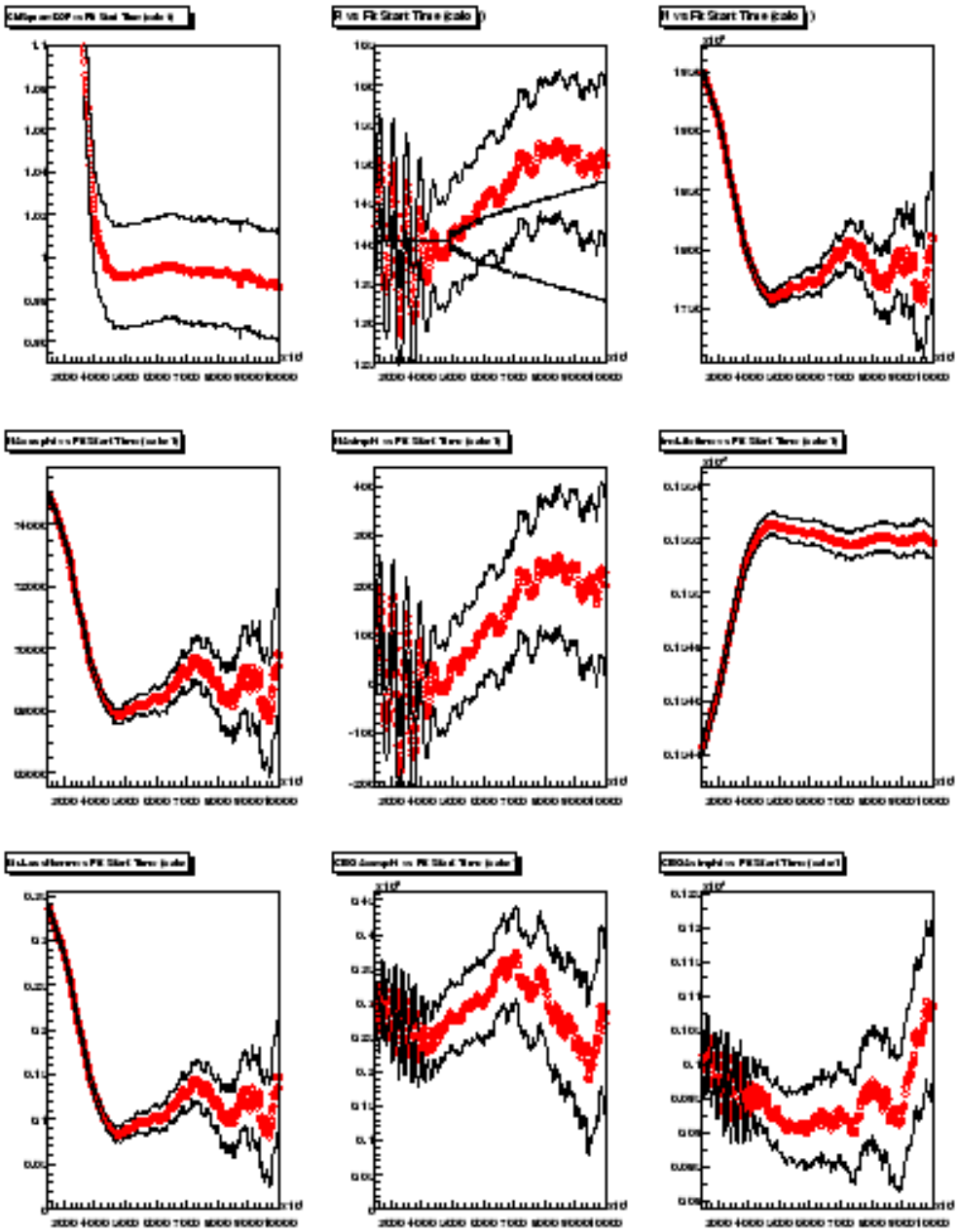

Figure 19. Results for the floated parameters for detector 1.

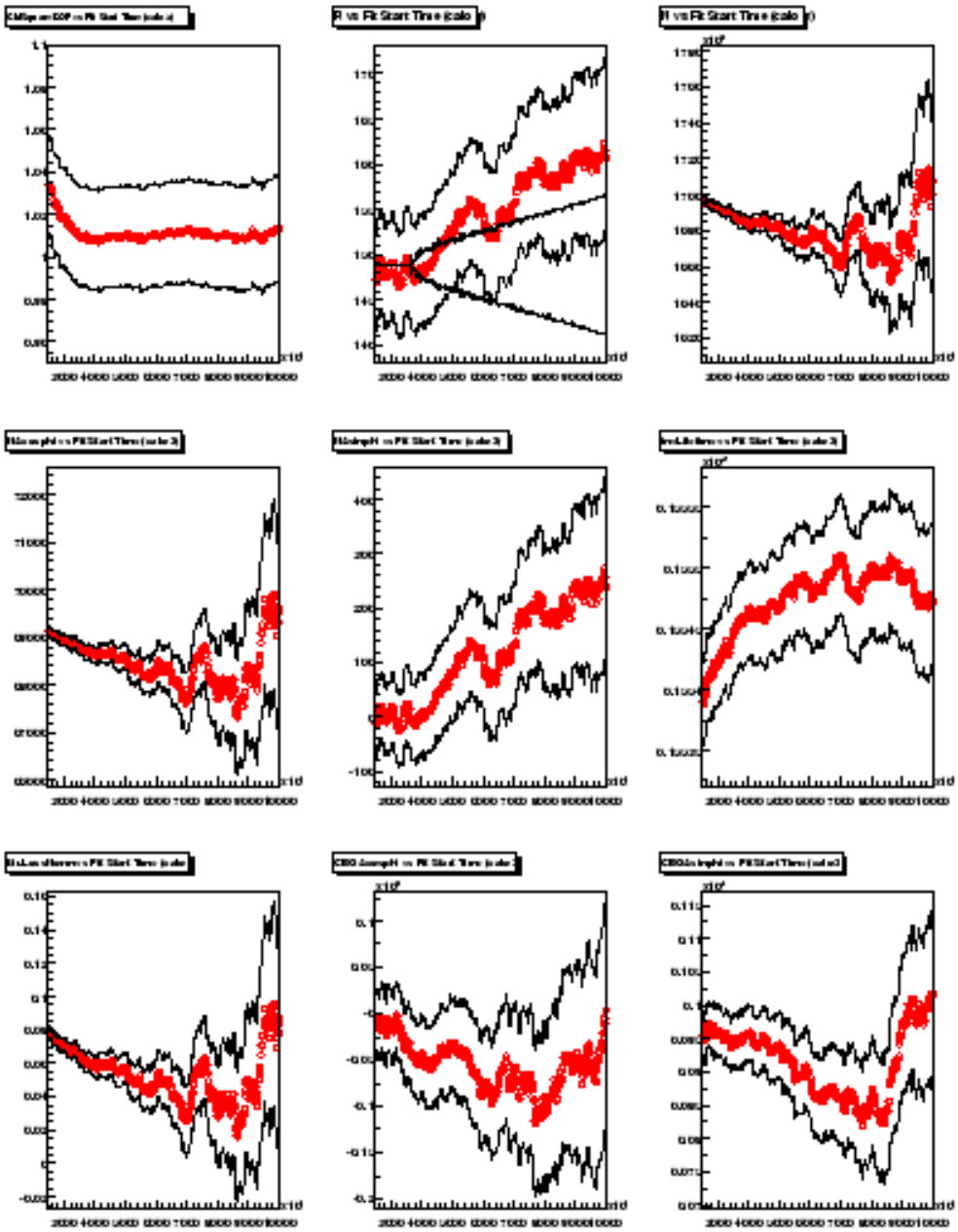

Figure 20. Results for the floated parameters for detector 3.